NASA TECHNICAL NOTE

NASA TN D-8506

NASA TN D-8506

DOWNSTREAM INFLUENCE OF SWEPT SLOT INJECTION IN HYPERSONIC TURBULENT FLOW

Jerry N. Hefner, Aubrey M. Cary, Jr., and Dennis M. Bushnell

Langley Research Center
Hampton, Va. 23665

NATIONAL AERONAUTICS AND SPACE ADMINISTRATION • WASHINGTON D. C. • AUGUST 1977

1. Report No.	2. Government Accession No.	3. Recipient's Catalog No.
NASA TN D-8506		

4. Title and Subtitle	5. Report Date
DOWNSTREAM INFLUENCE OF SWEPT SLOT INJECTION IN HYPERSONIC TURBULENT FLOW	August 1977
	6. Performing Organization Code

7. Author(s)	8. Performing Organization Report No.
Jerry N. Hefner, Aubrey M. Cary, Jr., and Dennis M. Bushnell	L-11464
	10. Work Unit No. 505-06-15-03

9. Performing Organization Name and Address	11. Contract or Grant No.
NASA Langley Research Center Hampton, VA 23665	
	13. Type of Report and Period Covered
12. Sponsoring Agency Name and Address	Technical Note
National Aeronautics and Space Administration Washington, DC 20546	14. Sponsoring Agency Code

15. Supplementary Notes

16. Abstract

Results of an experimental and numerical investigation of tangential swept slot injection (sweep angles of 22.5° and 45°) into a thick turbulent boundary layer at Mach 6 are presented. Film cooling effectiveness, skin friction, and flow structure downstream of the swept slot injection are investigated. The data are compared with that for unswept slots, and it is found that cooling effectiveness and skin-friction reductions are not significantly affected by sweeping the slot. Predictions of cooling effectiveness and skin friction obtained by a numerical finite-difference technique agree reasonably well with experimental surface variables.

17. Key Words (Suggested by Author(s))	18. Distribution Statement
Slot injection Film cooling Skin-friction reduction Flow angle measurements Boundary-layer profiles	Unclassified - Unlimited Subject Category 34

19. Security Classif. (of this report)	20. Security Classif. (of this page)	21. No. of Pages	22. Price*
Unclassified	Unclassified	50	$4.00

* For sale by the National Technical Information Service, Springfield, Virginia 22161

DOWNSTREAM INFLUENCE OF SWEPT SLOT INJECTION IN HYPERSONIC TURBULENT FLOW

Jerry N. Hefner, Aubrey M. Cary, Jr., and
Dennis M. Bushnell
Langley Research Center

SUMMARY

Results of an experimental and numerical investigation of tangential swept slot injection (sweep angles of 22.5° and 45°) into a thick turbulent boundary layer at Mach 5 are presented. Film cooling effectiveness, skin friction, and flow structure downstream of the swept slot injection are investigated. The data are compared with that for unswept slots, and it is found that cooling effectiveness and skin-friction reductions are not significantly affected by sweeping the slot. Predictions of cooling effectiveness and skin friction obtained by a numerical finite-difference technique agree reasonably well with experimental surface variables.

INTRODUCTION

Surface temperatures of an uncooled hypersonic aircraft may reach very high temperatures and may dictate the use of hot structural concepts. Systems studies show that lighter and less expensive structural materials can be used if these operational surface temperatures can be reduced below the radiation equilibrium temperature (ref. 1). Film cooling provides one means of reducing these high operational surface temperatures. Experimental studies of tangential slot injection at Mach 6 (refs. 2 and 3) have shown that the film cooling in two-dimensional, high-speed turbulent flow is significantly more effective than that indicated by extrapolations of low-speed results to high-speed conditions. However, many practical applications of slot injection film cooling (particularly on wings) will probably require the slots to be swept relative to the surface streamline direction. Reference 4 presents heat-transfer results which indicate the combined effects of three-dimensionality and pressure gradient on film cooling on a cone at angle of attack. However, detailed studies have not been conducted to determine the effect of sweeping the slot relative to the inviscid streamlines on the film cooling effectiveness. Furthermore, it is important to determine whether the skin-friction reductions found for two-dimensional slot injection (ref. 5) could be realized for the three-dimensional turbulent flow downstream of swept slot injection. Therefore, the present investigation was conducted to determine both numerically and experimentally the effect of sweep on film cooling effectiveness, skin friction, and flow structure downstream of the slot.

The experimental data obtained in this investigation are important for evaluating slot injection film cooling as an active cooling technique. If these data indicate that three-dimensional slot injection film cooling is as effective

as the two-dimensional case, then systems studies would be appropriate to ascertain the merits of slot-cooled aircraft structures. In addition, these data provide a unique test case (that is, near zero pressure gradient and zero curvature external flow) for validating numerical three-dimensional turbulent boundary-layer solutions currently under development. The numerical and experimental information generated is also necessary for assessing other possible uses for slot injection such as inlet boundary-layer control (ref. 6), aerodynamic windows for gas dynamic lasers (ref. 7), and low-speed drag-reduction systems.

The present paper reports measurements at Mach 6 of surface equilibrium temperature (cooling effectiveness), skin friction, and boundary-layer profiles (pitot pressure, total temperature, and flow angle) downstream of two swept slots ($\Lambda = 22.5^\circ$ and $\Lambda = 45^\circ$). The experiments utilized sonic, tangential air injection into a thick turbulent boundary layer. Surface pressures and oil-flow data were obtained to aid in interpreting the flow structure downstream of the slot. The effects of slot height and injectant temperature on the swept slot cooling effectiveness are measured and discussed. The cooling effectiveness and skin friction as well as boundary-layer profiles downstream of the swept slots are compared with previous data for unswept slots. A finite-difference solution developed for unswept tangential slot injection (ref. 8) was modified to account for swept slot injection, and predictions obtained by this technique are compared with the experimental data.

SYMBOLS

A2	mixing-length ratio in mixing zone (see fig. 4(a) and ref. 8)
C_f	skin-friction coefficient, τ_w/q
D	diameter
I	electrical current
M	Mach number
p	pressure
q	dynamic pressure, $\frac{1}{2}\rho u^2$
R	wire resistance
S	slot height
T	temperature
t	slot lip thickness (0.159 cm)
u	velocity in free-stream direction

u_N velocity perpendicular to slot

x distance downstream of slot parallel with free stream

y distance above surface, downstream of slot

y' distance above top of slot lip, $y - S - t$

δ boundary-layer velocity thickness (at $u/u_\infty \approx 0.995$)

ϵ cooling effectiveness parameter, $\dfrac{T_{t,\infty} - T_{eq}}{T_{t,\infty} - T_{t,j}}$

θ surface streamline direction measured from streamline parallel to free-stream direction in plane of flat plate (see fig. 1)

Λ slot sweep angle in plane of flat plate (see fig. 1)

λ mass flow parameter, $\dfrac{\rho_j u_{N,j}}{\rho_\infty u_\infty}$

μ viscosity

ρ density

τ_w component of shear stress in free-stream direction

ϕ wire output function (see fig. 3)

Subscripts:

eq equilibrium

j slot

o without slot

p probe

t total or stagnation

w wall

w_1, w_2 wire 1 and wire 2, respectively

∞ free stream

DESCRIPTION OF INVESTIGATION

Experimental Investigation

Facility and model.- The experimental investigation was conducted in the Langley 20-inch Mach 6 tunnel (see appendix of ref. 9 for a description of the tunnel) at a free-stream total temperature and unit Reynolds number per centimeter of 492 K and 0.287×10^6, respectively. The model (see fig. 1) was an epoxy resin fiberglass flat plate (35.5 cm wide and 91.4 cm long) with end plates and was mounted parallel with and recessed below the flat tunnel wall. The slot flow was injected tangentially over the surface of the flat plate from a two-dimensional sonic slot swept at either 22.5° or 45° relative to the free-stream flow direction. The slot flow was injected normal to the slot face and the local flow angle at the slot was therefore 22.5° or 45° relative to the free-stream flow. An example of the surface flow development downstream of the 45° swept slot is shown in figure 2 where the sketched streamlines were obtained from experimental surface oil-flow studies. The surface flow is normal to the slot face near the slot and gradually turns parallel with the free-stream direction further downstream. The slot configuration was identical to that used in references 3 and 5 and could be adjusted to provide slot heights S of 0.159, 0.476, and 1.111 cm and the lip thickness t was held constant at 0.159 cm. The slot mass flow rate $\rho_j u_{N,j}$, found to be uniform over a midspan of at least 20 cm in reference 5, was varied to insure that the velocity at the slot exit was sonic. The ratio of measured slot mass flow rate to calculated free-stream mass flow rate ($\lambda = \rho_j u_{N,j}/\rho_\infty u_\infty$) ranged from 0.042 to 0.838. The temperature of the slot flow was controlled by using a liquid nitrogen heat exchanger and for this investigation was varied from 136 K to 311 K.

Surface measurements.- Plate surface temperatures were measured along the center line by flush-mounted thermocouples and skin friction was measured by floating element gages located 6.36 cm off center line. Pressure orifices were located at the slot exit and nominally 3.81 cm off center line at several downstream x-locations.

A plate surface temperature was considered to be in equilibrium when it changed less than 0.1 percent over a time interval of 100 seconds. This criterion, although arbitrary, should provide sufficiently accurate values of equilibrium surface temperature. Generally, only the forward portion of the plate surface ($x < 65$ cm) reached equilibrium temperature in the available test time ($\approx$1800 sec).

The null-type skin-friction balances used in this study employed a floating element with a diameter of 0.94 cm and a surrounding gap width of 0.01 cm; the axes of the balances were alined with the free-stream flow. The balances had multiple sensitivities of 0.15 g/cm^2, 1.5 g/cm^2, and 15 g/cm^2 and were statically calibrated before and after the test program by applying a known load and measuring the voltage necessary to null the balance. The calibration remained constant throughout the tests within 3 percent of the measured value. Water-cooled jackets were used to maintain the balance internal temperature below 360 K at all times; thus, experimental errors due to temperature sensitivity of the balance coil were significantly reduced.

A mixture of silicon oil and lampblack was distributed in random dots of various sizes over the surface of the model to study the surface streamline patterns. Motion pictures (35 mm) were taken of the oil-flow patterns during the tests. Surface flow angles were measured graphically from the oil-flow patterns photographed during the run. The surface streamlines indicated that the flow exited normal to the slot as shown in figure 2.

Probe measurements.- Surface and pitot pressures were measured by multi-range capacitance-type pressure transducers calibrated to better than 1-percent full-scale accuracy on each range. The tip of the pitot probe was 0.046 cm high and 0.198 cm wide; the total temperature probe was a shielded thermocouple with base bleed and a circular tip of 0.191 cm diameter. The temperature probe was calibrated for the conditions of the present tests and was found to have a recovery factor of 0.99. Based on the extensive calibrations of a similar probe over a wider range of Reynolds number and Mach number (ref. 5), this recovery factor was assumed to be valid for the present study and was used to correct the total temperature probe data. Velocities were calculated by using the corrected probe values of temperature and the measured pitot pressure along with the assumption of constant static pressure across the boundary layer.

Flow angle measurements.- Boundary-layer flow angle measurements were obtained 5.40 cm downstream of the 22.5° swept slot and 8.26 cm downstream of the 45° swept slot by using a swept, dual hot-wire probe (fig. 3) similar to that used in reference 10. The hot-wire probe was constructed from two small spirals of platinum-iridium wire, each stretched across and silver-soldered to notched needles. Platinum-iridium wire was used instead of the more conventional copper-plated tungsten wire because of the high temperatures and oxidation problems of the present tests. Also the wire was stretched into a loose spiral rather than a tightly wound coil and provided the necessary strength for the rather high dynamic pressures of the Mach 6 wind-tunnel facility. The wire diameter was 0.0025 cm and the ratio of wire length to wire diameter was 110. The probe was calibrated in the Mach 6 free stream by setting the probe at known yaw angles and measuring the probe output. (See calibration curve in fig. 3(b).) The probe was calibrated so that the response was essentially independent of local Reynolds number and Mach number.

Numerical Investigation

A numerical finite-difference solution procedure for tangential slot injection into supersonic turbulent boundary layers (ref. 8) was modified to account for swept slot injection by including the spanwise momentum equation in the solution. (See refs. 11 and 12 for a description of the swept slot code without the slot injection eddy viscosity option, which was modeled after ref. 8.) The present calculation is therefore essentially a combination of the capabilities existing in references 8, 11, and 12. The three-dimensional turbulence model used was the "invariant turbulence" or scalar eddy viscosity approach discussed in references 11 and 12. This approach uses the usual bounday-layer approximation of constant static pressure in the direction normal to the surface.

RESULTS AND DISCUSSION

Flow Structure and Surface Pressure Distribution

The slot flow field is schematically shown in figure 4(a) for the case of nearly "matched" pressure conditions. Ideally, the "matched" pressure condition refers to the case where the slot and free-stream static pressure are equal and the static pressure along the wall is nearly constant ($p_w/p_{w,o} \approx 1$). As shown in figure 4(b), this condition cannot be fully realized in the region very close to the slot exit ($x/S \approx 0.6$) unless the slot flow is allowed to expand fully; the fuly expanded slot flow would match the static pressure in the immediate vicinity of the slot with the free-stream static pressure, but would generate pressures lower than the stream static pressure further downstream of the slot (ref. 5). Figure 4(b) shows that as the mass flow rate λ was increased from the no-injection case, the wall static pressure in the slot region increased until the slot flow became sonic; at this point the slot pressure was slightly less than the stream static pressure $p_{w,o}$ because of the expansion of the free-stream flow over the slot lip. (See fig. 4(a).) Further increasing the slot mass flow rates first reduced the near slot pressures and then increased them. This subsequent increase in the near slot pressure is caused by the slot fully expanding; the Mach number distribution in the near slot region remains constant. Since the present investigation is primarily concerned with the case where the slot flow is sonic and the downstream pressure gradient is as small as possible, most of the slot mass flow rates are at near "matched" pressure conditons (that is, where the slot flow just becomes sonic and the near slot pressures are somewhat less than the stream static pressure).

Surface static pressures measured at seven streamwise locations downstream of the 22.5° swept slot and eight streamwise locations downstream of the 45° swept slot are shown in figures 4(c) and 4(d), respectively, for the three slot heights at near "matched" pressure conditions. The wall static pressure p_w is normalized by the measured stream static pressure with no slot $p_{w,o}$. Although an adverse pressure gradient exists close to the slot exit, the surface pressures further downstream of the slot are very near free-stream static pressure in all cases.

Cooling Effectiveness

A summary of the equilibrium temperatures for near "matched" pressures downstream of the swept slots (Λ = 22.5° and 45°) for $T_{t,j}/T_{t,\infty} \approx 0.6$ and 0.32 is presented in figures 5 and 6 in a form which correlated effectiveness data in references 2, 3, and 5. The distance parameter $(x/S)\lambda^{-0.8}$, which is based on the chordwise distance downstream of the slot (parallel with the mainstream flow direction) correlates the effectiveness data for both slot flow temperatures in a relatively narrow band for the slot mass flow rates and slot heights of the present investigation. Note that the data appear to correlate at a given slot flow total temperature, but the correlation is different for the two different slot temperature levels. The data appear to correlate as long as λ is changed by changing the ratios of slot density to free-stream density; if the ratio of slot velocity to the free-stream velocity is changed, the correlation also changes. (Compare figs. 5 and 6.) Table I presents coefficients

for the straight-line correlations of the swept slot data shown in figures 5 and 6 as well as those for the unswept slot data of reference 5 for similar total temperature ratios and mass flow rates.

The effect of slot sweep on the film cooling effectiveness is clearly seen in figures 5 and 6. Although the cooling effectiveness is lower and decreases more rapidly for the cooler slot flow temperature ($T_{t,j}/T_{t,\infty} \approx 0.32$), the film cooling effectiveness for the swept slots decreases only slightly below that for the comparable unswept slots for both sweep angles and both slot flow temperatures. However, theoretically the total cooled area downstream of the swept slot is reduced by cosine Λ when compared with the unswept slot; the oil-flow studies tend to confirm this condition. (For example, fig. 2 shows that the streamlines downstream of the swept slot remain parallel as the slot flow mixes with the stream boundary layer and turns toward the free-stream direction.) As was found in reference 5 for the unswept slots, the cooling effectiveness for the swept slots for $(x/S)\lambda^{-0.8} < 100$ is less than the expected value of $\epsilon = 1$ because of heat conduction from the free-stream flow through the metal slot lip and into the slot flow.

Cooling effectiveness data for mass flow rates greater than the near "matched" pressure condition are shown in figure 7 for the 22.5° swept slot with $T_{t,j}/T_{t,\infty} \approx 0.6$ and 0.45. The straight-line correlations of the data shown in figures 5 and 6 and table I are shown for comparison with the data for the more fully expanded slot flows. The higher mass flow rates slightly increase the effective cooling lengths (that is, the distance downstream of slot where $\epsilon \approx 1.0$) for the 22.5° swept slot; however, the rate of decrease in effectiveness beyond this cooling length is approximately the same as that found for near "matched" pressure conditions. Since sweeping the slot has only a minor influence on effectiveness ($\Lambda \leq 45°$), the favorable effects of slot injection in high-speed flow are retained. (See refs. 3 and 5.)

Skin Friction

Local surface skin-friction measurements presented in terms of $C_f/C_{f,o}$ are shown for $T_{t,j}/T_{t,\infty} \approx 0.6$ in figure 8 for both sweep angles and the three slot heights. Skin-friction data downstream of the unswept slot (ref. 5) at similar test conditions are shown in the figure for comparison. Skin-friction data for the swept slots at $T_{t,j}/T_{t,\infty} \approx 0.32$ were not obtained in the present study since reference 5 showed that decreasing the slot flow temperature had a negligible effect on the skin friction even though the cooling effectivenes was significantly reduced. Sweeping the slot reduces the measured skin friction downstream of the slot below that for the unswept two-dimensional slot for the three slot heights investigated; therefore, the significant reductions in skin friction found for the unswept slot (ref. 5) were also found for the swept slots.

Comparison of Finite-Difference Predictions With Experiment

Surface parameters.- The implicit finite-difference solution procedure developed for tangential slot injection into supersonic turbulent boundary layers (ref. 8) was modified to predict the flow downstream of swept slot

injection. Initial slot and boundary-layer profiles normal to the slot face were required as inputs into the numerical technique and were obtained experimentally for the largest slot height (S = 1.111 cm) for both the 22.5° and 45° swept slots (shown by the solid curves in fig. 9). Initial slot profiles were measured for both $T_{t,j}/T_{t,\infty} \approx 0.6$ and 0.32 for the 22.5° swept slot, whereas only the profiles for $T_{t,j}/T_{t,\infty} \approx 0.6$ were measured for the 45° swept slot. The slot velocity profiles obtained from measurements near the lower slot wall were modified for some calculations in an attempt to ascertain the effect of a "laminar-like" slot velocity profile on the downstream flow predictions; the measured slot velocity profiles near the lower wall are subject to interpretation because of possible probe interference effects. Also a laminar slot flow boundary layer may have occurred since the slot Reynolds number ($\rho_j u_{N,j} S/\mu_j$) was near transitional (approximately 3×10^3) and the slot flow was rapidly accelerated just prior to being injected (ref. 5). The stream or external boundary-layer profile shapes are typical of nozzle wall turbulent boundary layers, and the velocity thickness δ was approximately 4.5 cm. (See table II for a tabulation of the measured nozzle wall profiles.) The calculation was carried out in a coordinate system normal to the slot face. The external spanwise flow (assumed to be invariant in planes parallel to the slot face) was input from a vector decomposition of the measured tunnel wall boundary-layer profile.

As was discussed previously, a pressure gradient existed near the slot even for the nearly "matched" pressure condition. The effect of this gradient was explored numerically; the most "severe" pressure gradients that could be input into the swept slot program without causing flow separation are shown as unbroken fairings in figure 10 for the swept slots. It is readily seen that the maximum dp/dx used in the calculation is much less than local values indicated by the experimental data. (See section on "Flow Structure and Surface Pressure Distribution" for an explanation of these pressure gradients.) Therefore, based upon these calculations and careful study of the oil flow near the slot, it is tentatively concluded that the low velocity flow from the slot is locally separated for this slot height. However, the influence of this separation on surface shear and temperature seems to quickly "wash out" downstream. Limited numerical predictions were also obtained with a reduced mixing-length ratio (A2) for the free mixing region downstream of the slot lip. (See ref. 8 for a detailed discussion of the role of A2 in the eddy viscosity model.) The reason for varying this parameter will be discussed in connection with the downstream profile comparisons.

Cooling effectiveness and skin-friction predictions are compared with the experimental results in figures 11 and 12, respectively. The laminar slot predictions with zero pressure gradient and the turbulent slot predictions both with and without the adverse pressure gradient for a mixing-length ratio (A2) of 0.09 predict reasonably well the measured effectiveness and skin-friction data for the 22.5° swept slot for $T_{t,j}/T_{t,\infty} \approx 0.6$. The laminar slot predictions for the 22.5° swept slot with the adverse pressure gradient were not obtained since the prediction technique indicated that the input pressure gradient was too severe for the laminar slot flow and with even the moderate dp/dx shown in figure 10 forced the slot flow to separate locally. Decreasing the mixing-length ratio for the free mixing region from 0.09 to 0.06 for the laminar slot without pressure gradient adversely affects the agreement between

the predicted and measured cooling effectiveness but enhanced the agreement between the predicted and measured skin friction downstream of the slot. (See fig. 12(a) for $x/S > 10$.) For the 45° swept slot, only the predictions for the laminar slot flow with pressure gradient and with a reduced mixing-length ratio ($A2 = 0.06$) gave reasonable agreement with the cooling effectiveness and skin-friction data. Limited attempts to predict the cooling effectiveness data for the cooler slot flow temperature ($T_{t,j}/T_{t,\infty} \approx 0.32$) for the 22.5° swept slot (fig. 11(c)) indicated fair agreement between the predictions and the data. The comparison of the predicted and measured effectiveness for the warmer slot flow ($T_{t,j}/T_{t,\infty} \approx 0.6$) appeared to indicate that the pressure gradient did not significantly affect the downstream calculations; therefore, the cooler slot flow calculations were conducted only for a zero pressure gradient.

Profile and flow angle comparisons.- Although the finite-difference calculations investigated do provide reasonable predictions of the trends and approximate magnitudes of the measured cooling effectiveness and skin-friction data, these same calculations fail to predict the velocity and total temperature profiles near the plate wall ($y < 2$ cm) at downstream x-locations where the slot flow has turned parallel with the stream direction. (See figs. 13 and 14.) Also, predictions of the flow angle through the viscous region are very poor compared with the experimental data. (See fig. 15.) The measured velocity profiles presented in figure 13 and table III for both swept slots show a concave velocity profile near the plate wall. This is not a three-dimensional effect since velocity profiles recently obtained in the present investigation downstream of the two-dimensional slot configuration of references 3 and 5 (fig. 13(a) and tables III(a) and III(b)) are similarly shaped. Furthermore, this anomaly was also found in the two-dimensional slot injection studies of references 13 and 14. Reducing the mixing-length ratio for the free mixing length region downstream of the slot proved to be partially effective in achieving agreement between predicted velocity profiles and measured profiles in references 13 and 14. In the present investigation, reducing the mixing-length ratio did have a favorable influence on the prediction of the measured velocity profiles, but made the already poor predictions of the measured surface flow angles (from oil flow) and flow angle profiles (from swept hot-wire probe) even worse. (See figs. 15 and 16.) It is believed that one plausible reason that the surface flow turns more rapidly than predicted is that the slot flow separates locally in the region very near the slot exit. Figure 16 shows that the predicted rate of surface flow turning (the change in θ with respect to x) downstream of the region where the slot flow remains perpendicular to the slot appears to agree reasonably well with $d\theta/dx$ from the experimental results.

The comparison of the present swept and unswept slot finite-difference predictions with experimental profiles (figs. 13, 14, and 15) and similar comparisons for two-dimensional slot injections in reference 14 show that the present understanding of the turbulent mixing which occurs for slot injection into a thick supersonic/hypersonic turbulent boundary layer is insufficient. The present calculations tend to suggest that (a) the input pressure gradient is only important near the slot and tends to disappear 20 to 40 slot heights downstream and (b) the concave velocity profiles indicate either a "laminar-like" mixing region or the influence of the adverse experimental pressure gradient which was considerably larger than could be included in a "boundary-layer"

method. (See fig. 10.) However, for the two-dimensional slot flow case, recent improved turbulence modeling research, reported in reference 15, indicates very good agreement with the $M_\infty = 6$ profiles shown in figures 13(a) and 14(a).

CONCLUSIONS

The present data, consisting of (1) adiabatic wall temperature distributions, (2) direct skin-friction measurements, (3) surface flow angles, (4) three-dimensional turbulent flow profiles, and (5) surface pressure distributions over a range of sweep angle, slot height, slot mass flow rate, and slot total temperature comprise a fairly complete and definitive study of the influence of three-dimensionality upon tangential slot injection. In addition, the paper presents results of a new three-dimensional calculation method for slot injection. Major conclusions resulting from the present experimental and numerical investigation are as follows:

1. The large film cooling effectiveness found for unswept slots at supersonic/hypersonic speeds was not significantly affected by sweeping the slot to 22.5° and 45° for either $T_{t,j}/T_{t,\infty} \approx 0.6$ or 0.32. In agreement with the two-dimensional case, the film cooling effectiveness downstream of the swept slots decreased when the ratio of the slot to free-stream total temperature $T_{t,j}/T_{t,\infty}$ was reduced from 0.6 to 0.32. For the range of slot heights investigated, slot height did not significantly affect the swept slot cooling effectiveness correlation.

2. The large reductions in local surface skin friction measured downstream of unswept slots still occurred as the sweep angle was increased for all slot heights investigated.

3. Predictions of the film cooling effectiveness and skin friction obtained by a numerical technique agree reasonably well with the measured results for both sweep angles.

4. The swept slot finite-difference solution with the simple "invariant turbulence" or scalar eddy viscosity model fails to predict the downstream velocity, total temperature, and flow angle profiles in the inner or slot mixing region. This disagreement is tentatively ascribed to the existence of a localized three-dimensional separation of the slot flow immediately downstream of the slot exit which allows the near wall flow to turn prematurely under the action of pressure forces.

Langley Research Center
National Aeronautics and Space Administration
Hampton, VA 23665
June 2, 1977

REFERENCES

1. Becker, John V.; and Kirkham, Frank S.: Hypersonic Transports. Vehicle Technology for Civil Aviation - The Seventies and Beyond. NASA SP-292, 1971, pp. 429-445.

2. Parthasarathy, K.; and Zakkay, V.: An Experimental Investigation of Turbulent Slot Injection at Mach 6. AIAA J., vol. 8, no. 7, July 1970, pp. 1302-1307.

3. Cary, Aubrey M., Jr.; and Hefner, Jerry N.: Film Cooling Effectiveness in Hypersonic Turbulent Flow. AIAA J., vol. 8, no. 11, Nov. 1970, pp. 2090-2091.

4. Zakkay, Victor; and Wang, Chi R.: Investigation of Multiple Slot Film Cooling to a Blunt Nose Cone. AIAA Paper No. 73-698, July 1973.

5. Cary, Aubrey M., Jr.; and Hefner, Jerry N.: Film-Cooling Effectiveness and Skin Friction in Hypersonic Turbulent Flow. AIAA J., vol. 10, no. 9, Sept. 1972, pp. 1188-1193.

6. Ogorodnikov, D. A.; Grin, V. T.; and Zakharov, N. N.: Boundary Layer Control of Hypersonic Air Inlets. NASA TT F-13,927, 1972.

7. Parmentier, E. M.: Supersonic Flow Aerodynamic Windows for High Power Lasers. AIAA Paper No. 72-710, June 1972.

8. Beckwith, Ivan E.; and Bushnell, Dennis M.: Calculation by a Finite-Difference Method of Supersonic Turbulent Boundary Layers With Tangential Slot Injection. NASA TN D-6221, 1971.

9. Goldberg, Theodore J.; and Hefner, Jerry N. (appendix by James C. Emery): Starting Phenomena for Hypersonic Inlets With Thick Turbulent Boundary Layers at Mach 6. NASA TN D-6280, 1971.

10. Fischer, Michael C.; and Weinstein, Leonard M.: Three-Dimensional Hypersonic Trasitional/Turbulent Mean Flow Profiles on a Slender Cone at Angle of Attack. AIAA Paper No. 73-635, July 1973.

11. Hixon, Barbara A.; Beckwith, Ivan E.; and Bushnell, Dennis M.: Computer Program for Compressible Laminar or Turbulent Nonsimilar Boundary Layers. NASA TM X-2140, 1971.

12. Hunt, James L.; Bushnell, Dennis M; and Beckwith, Ivan E.: The Compressible Turbulent Boundary Layer on a Blunt Swept Slab With and Without Leading-Edge Blowing. NASA TN D-6203, 1971

13. Kenworthy, Michael; and Schetz, Joseph A.: An Experimental Study of Slot Injection Into a Supersonic Stream. NASA CR-2128, 1973.

14. Miner, E. W.; and Lewis, C. H.: A Finite Difference Method for Predicting Supersonic Turbulent Boundary-Layer Flows With Tangential Slot Injection. NASA CR-2124, 1972.

15. Cary, A. M., Jr.; Bushnell, D. M.; and Hefner, J. N.: Slot Injection for Skin Friction Drag Reduction. AGARD/VKI Special Course "Concepts for Drag Reduction." AGARD-R-654, Apr. 1977.

TABLE I.- COOLING EFFECTIVENESS CORRELATIONS

FOR SWEPT SLOT INJECTION

$$\left[\epsilon = a\left[(x/S)\lambda - 0.6\right]^{-b}\right]$$

Λ, deg	$T_{t,j}/T_{t,\infty}$	a	b
0	0.63	2.76	0.226
22.5	.60	3.12	.263
45	.60	3.33	.269
0	.43	4.46	.360
22.5	.32	4.51	.390
45	.32	5.19	.393

TABLE II.- TABULATION OF MEASURED BOUNDARY-LAYER PROFILE AT SLOT

$\left[p_{t,\infty} = 3.50 \text{ MPa}; \quad T_w/T_{t,\infty} = 0.73\right]$

y', cm	$p_{t,p}$, kPa	$T_{t,p}$, K	M/M_∞	u/u_∞	$T_t/T_{t,\infty}$
0.084	9.032	394.4	0.280	0.576	0.800
.130	11.190	403.8	.319	.631	.819
.178	12.742	409.7	.343	.663	.831
.249	16.065	417.1	.388	.711	.846
.287	16.975	417.6	.400	.721	.847
.356	19.319	424.0	.427	.747	.860
.389	19.747	426.9	.432	.754	.866
.437	21.450	427.4	.451	.768	.867
.546	23.559	432.4	.474	.789	.877
.620	24.490	434.8	.484	.796	.882
.671	25.524	437.3	.494	804	.887
.726	26.531	439.8	.504	.812	.892
.795	28.289	444.2	.521	.826	.901
1.054	30.268	451.6	.540	.842	.916
1.191	32.943	455.0	.564	.857	.923
1.301	34.667	456.5	.579	.865	.926
1.425	37.514	459.5	.603	.878	.932
1.577	39.011	463.4	.613	.885	.940
1.702	42.920	465.9	.646	.900	.945
1.829	46.588	468.8	.674	.912	.951
2.068	49.815	473.3	.697	.923	.960
2.360	59.929	477.7	.767	.946	.969
2.583	67.189	480.7	.812	.958	.975
2.878	71.954	482.2	.841	.965	.978
3.198	77.642	483.1	.874	.972	.980
3.868	89.308	489.5	.937	.988	.993
4.519	99.057	492.0	.988	.998	.998
5.375	101.332	493.0	1.000	1.000	1.000

TABLE III.- TABULATION OF MEASURED BOUNDARY-LAYER PROFILES

(a) $\Lambda = 0^{\circ}$; $T_{t,j}/T_{t,\infty} = 0.6$; $\lambda = 0.047$;
$S = 1.111$ cm; $x = 10.8$ cm; $M_{\infty} = 6.05$;
$T_w/T_{t,\infty} = 0.64$; $p_{t,\infty} = 3.57$ MPa;
$T_{t,\infty} = 482.7$ K

y, cm	$p_{t,p}$, kPa	$T_{t,p}$, K	M/M_{∞}	u/u_{∞}	$T_t/T_{t,\infty}$
0.018	2.164	316.7	0.017	0.039	0.657
.084	2.468	↓	.074	.170	↓
.142	2.634		.091	.206	
.198	2.785		.102	.231	
.249	2.916	317.8	.111	.248	.659
.307	3.158	319.4	.126	.279	.663
.371	3.447	323.3	.140	.310	.671
.462	3.806	330.6	.155	.342	.686
.488	4.116	332.2	.167	.364	.689
.533	4.537	336.1	.179	.387	.697
.589	4.930	341.7	.192	.413	.709
.640	5.433	346.7	.205	.438	.719
.660	5.674	348.3	.210	.447	.722
.719	6.281	355.6	.225	.476	.738
.795	7.322	363.9	.248	.516	.755
.838	8.053	368.3	.263	.540	.764
.884	8.701	375.0	.274	.560	.778
.960	10.128	384.4	.299	.599	.798
1.039	11.542	393.9	.322	.633	.817
1.062	12.162	396.7	.331	.645	.823
1.118	13.231	401.7	.347	.666	.833
1.173	14.761	406.7	.369	.691	.844
1.217	15.196	411.1	.374	.700	.853
1.300	17.037	418.3	.398	.728	.868
1.575	22.105	430.6	.456	.783	.893
1.925	26.345	440.0	.499	.818	.912
2.636	35.232	450.6	.582	.870	.934
3.101	43.120	456.7	.645	.900	.947
3.816	51.966	465.0	.709	.928	.964
4.412	67.789	470.6	.812	.958	.976
5.667	96.230	477.8	.968	.991	.991
6.401	100.946	480.6	.993	.997	.997
6.807	101.863	481.1	.998	.998	.998
7.640	102.401	482.2	1.000	1.000	1.000

TABLE III.- Continued

(b) $\Lambda = 0^{\circ}$; $T_{t,j}/T_{t,\infty} = 0.6$; $\lambda = 0.047$;
$S = 1.111$ cm; $x = 27.6$ cm; $M_{\infty} = 6.04$;
$T_w/T_{t,\infty} = 0.67$; $p_{t,\infty} = 3.56$ MPa;
$T_{t,\infty} = 486.1$ K

y, cm	$p_{t,p}$, kPa	$T_{t,p}$, K	M/M_{∞}	u/u_{∞}	$T_t/T_{t,\infty}$
0.028	3.992	335.7	0.162	0.356	0.690
.081	5.468	336.7	.207	.433	.693
.132	6.177	339.4	.224	.460	.698
.185	6.598	346.7	.233	.480	.713
.229	6.888	351.1	.238	.491	.722
.295	7.343	355.6	.248	.508	.732
.307	7.460	356.7	.252	.514	.734
.384	7.686	361.1	.260	.528	.743
.442	8.232	364.4	.267	.540	.750
.495	8.556	367.8	.272	.549	.756
.551	8.991	370.6	.280	.561	.762
.592	9.246	374.4	.283	.569	.770
.643	9.763	376.1	.293	.582	.774
.693	10.135	380.6	.300	.594	.783
.752	10.908	384.4	.313	.613	.791
.770	11.507	385.6	.322	.622	.794
.841	11.928	388.9	.328	.632	.800
.899	12.624	393.3	.339	.643	.809
.958	13.100	397.8	.346	.654	.818
1.034	14.334	402.8	.362	.679	.829
1.115	15.141	408.3	.373	.693	.840
1.173	15.610	411.1	.379	.702	.846
1.257	17.464	416.7	.404	.728	.857
1.303	18.050	418.3	.411	.735	.861
1.681	23.980	434.4	.477	.796	.894
1.941	27.758	440.0	.517	.824	.905
2.639	37.583	455.6	.603	.880	.937
3.185	44.968	469.4	.661	.914	.965
3.960	58.895	476.7	.752	.947	.980
4.448	66.141	480.0	.802	.962	.987
5.144	75.539	483.3	.866	.978	.994
5.796	84.585	484.4	.911	.986	.996
6.596	86.902	485.0	.917	.988	.998
7.760	101.877	486.1	1.000	1.000	1.000

TABLE III.- Continued

(c) $\Lambda = 22.5^{\circ}$; $T_{t,j}/T_{t,\infty} = 0.6$; $\lambda = 0.042$;
$S = 1.111$ cm; $x = 21$ cm; $M_{\infty} = 6.01$;
$T_w/T_{t,\infty} = 0.67$; $p_{t,\infty} = 3.65$ MPa;
$T_{t,\infty} = 495$ K

y, cm	$p_{t,p}$, kPa	$T_{t,p}$, K	M/M_{∞}	u/u_{∞}	$T_t/T_{t,\infty}$
0.036	3.006	342.1	0.106	0.243	0.691
.050	3.365	343.0	.127	.287	.693
.090	3.882	346.0	.151	.334	.699
.160	4.213	348.5	.163	.359	.704
.220	4.468	351.0	.172	.375	.709
.250	4.592	351.9	.175	.383	.711
.290	4.730	354.4	.179	.391	.716
.340	4.971	358.4	.186	.405	.724
.370	5.157	359.9	.191	.415	.727
.390	5.274	361.4	.194	.421	.730
.460	5.654	365.3	.204	.440	.738
.520	5.957	369.8	.211	.455	.747
.580	6.405	373.7	.221	.474	.755
.630	6.833	377.2	.228	.486	.762
.690	7.364	380.7	.241	.508	.769
.740	7.832	384.1	.250	.524	.776
.800	8.591	389.6	.265	.547	.787
.860	9.322	395.0	.278	.569	.798
.940	10.184	401.0	.291	.591	.810
.990	10.942	405.9	.304	.610	.820
1.04	11.804	410.9	.318	.630	.830
1.10	12.638	416.8	.329	.648	.842
1.21	14.141	423.7	.351	.690	.856
1.25	14.617	425.7	.356	.683	.860
1.31	16.361	430.7	.379	.709	.870
1.56	20.905	444.0	.433	.765	.897
1.84	25.690	453.4	.481	.808	.916
2.64	37.321	471.2	.584	.877	.952
3.21	44.471	477.7	.639	.904	.965
3.61	52.862	480.6	.699	.927	.971
4.35	65.417	485.1	.779	.952	.980
5.17	79.014	490.1	.857	.974	.990
5.71	84.757	492.0	.889	.979	.994
6.44	99.760	493.0	.965	.991	.996
7.06	107.186	495.0	1.000	1.000	1.000

TABLE III.- Continued

(d) $\Lambda = 45^{\circ}$; $T_{t,j}/T_{t,\infty} = 0.6$; $\lambda = 0.048$;
$S = 1.111$ cm; $x = 23$ cm; $M_{\infty} = 6.0$;
$T_w/T_{t,\infty} = 0.66$; $p_{t,\infty} = 3.56$ MPa;
$T_{t,\infty} = 498$ K

y, cm	$p_{t,p}$, kPa	$T_{t,p}$, K	M/M_{∞}	u/u_{∞}	$T_t/T_{t,\infty}$
0.036	2.916	339.4	0.094	0.216	0.681
.064	3.282	339.9	.118	.266	.682
.132	3.682	341.4	.135	.302	.685
.198	3.909	344.3	.148	.327	.691
.277	4.130	346.3	.156	.344	.695
.338	4.330	348.8	.163	.358	.700
.406	4.661	351.8	.173	.379	.706
.457	4.778	354.3	.177	.386	.711
.513	5.054	356.8	.184	.401	.716
.566	5.302	358.8	.191	.414	.720
.625	5.599	362.3	.198	.428	.727
.673	6.067	365.8	.210	.484	.734
.719	6.226	369.3	.213	.457	.741
.790	6.833	372.3	.227	.480	.747
.841	7.067	376.7	.231	.490	.756
.879	7.564	379.2	.241	.507	.761
.930	8.081	383.7	.251	.524	.770
.980	8.412	388.2	.257	.536	.779
1.056	9.156	395.2	.271	.559	.793
1.090	9.094	398.7	.269	.560	.800
1.128	9.756	402.2	.280	.577	.807
1.153	10.335	404.6	.290	.591	.812
1.230	11.121	411.1	.302	.612	.825
1.280	11.514	415.1	.308	.622	.833
1.488	14.948	427.6	.356	.684	.858
1.976	23.153	449.5	.450	.782	.902
2.586	34.646	464.4	.555	.857	.932
3.205	44.023	473.4	.628	.897	.950
3.890	57.289	481.9	.718	.933	.967
4.390	68.575	484.9	.787	.952	.973
5.230	92.679	489.9	.917	.982	.983
5.750	104.973	492.4	.977	.992	.988
6.540	105.697	498.3	1.000	1.000	1.000

TABLE III.- Concluded

(e) Λ = 22.5; $T_{t,j}/T_{t,\infty}$ = 0.32; λ = 0 061;
x = 21 cm; M_∞ = 6.0; $T_w/T_{t,\infty}$ = 0.52;
$p_{t,\infty}$ = 3.57 MPa; $T_{t,\infty}$ = 491.7 K

y, cm	$p_{t,p}$, kPa	$T_{t,p}$, K	M/M_∞	u/u_∞	$T_t/T_{t,\infty}$
0.023	2.744	256.2	0.087	0.177	0.520
.070	3.447	256.2	.132	.259	.520
.130	3.716	256.2	.144	.278	.521
.180	3.882	256.2	.151	.289	.520
.230	4.033	257.1	.157	.300	.523
.270	4.185	259.6	.162	.310	.528
.310	4.337	261.6	.167	.319	.532
.380	4.585	266.0	.175	.334	.541
.440	4.854	271.4	.183	.350	.552
.540	5.309	280.2	.195	.374	.570
.590	5.647	286.2	.204	.391	.582
.680	6.254	295.0	.218	.419	.600
.750	6.874	304.8	.232	.444	.620
.810	7.398	312.2	.242	.464	.635
.900	8.205	323.0	.258	.493	.657
.960	8.887	331.9	.270	.515	.675
1.05	10.011	343.2	.290	.548	.698
1.08	10.708	347.1	.301	.564	.706
1.15	11.438	357.9	.312	.585	.728
1.20	12.018	364.8	.322	.601	.742
1.25	12.700	372.2	.331	.617	.757
1.29	13.817	381.0	.347	.641	.775
1.58	17.582	415.5	.395	.715	.845
1.95	25.414	436.6	.480	.795	.888
2.56	34.439	456.8	.562	.839	.929
3.20	45.802	467.1	.650	.904	.950
3.84	57.447	473.5	.730	.935	.963
4.49	68.086	478.4	.797	.956	.973
5.12	82.875	482.8	.880	.975	.982
5.76	91.480	488.2	.925	.989	.993
6.37	98.298	491.7	.959	.996	1.000
7.04	105.895	491.7	1.000	1.000	1.000

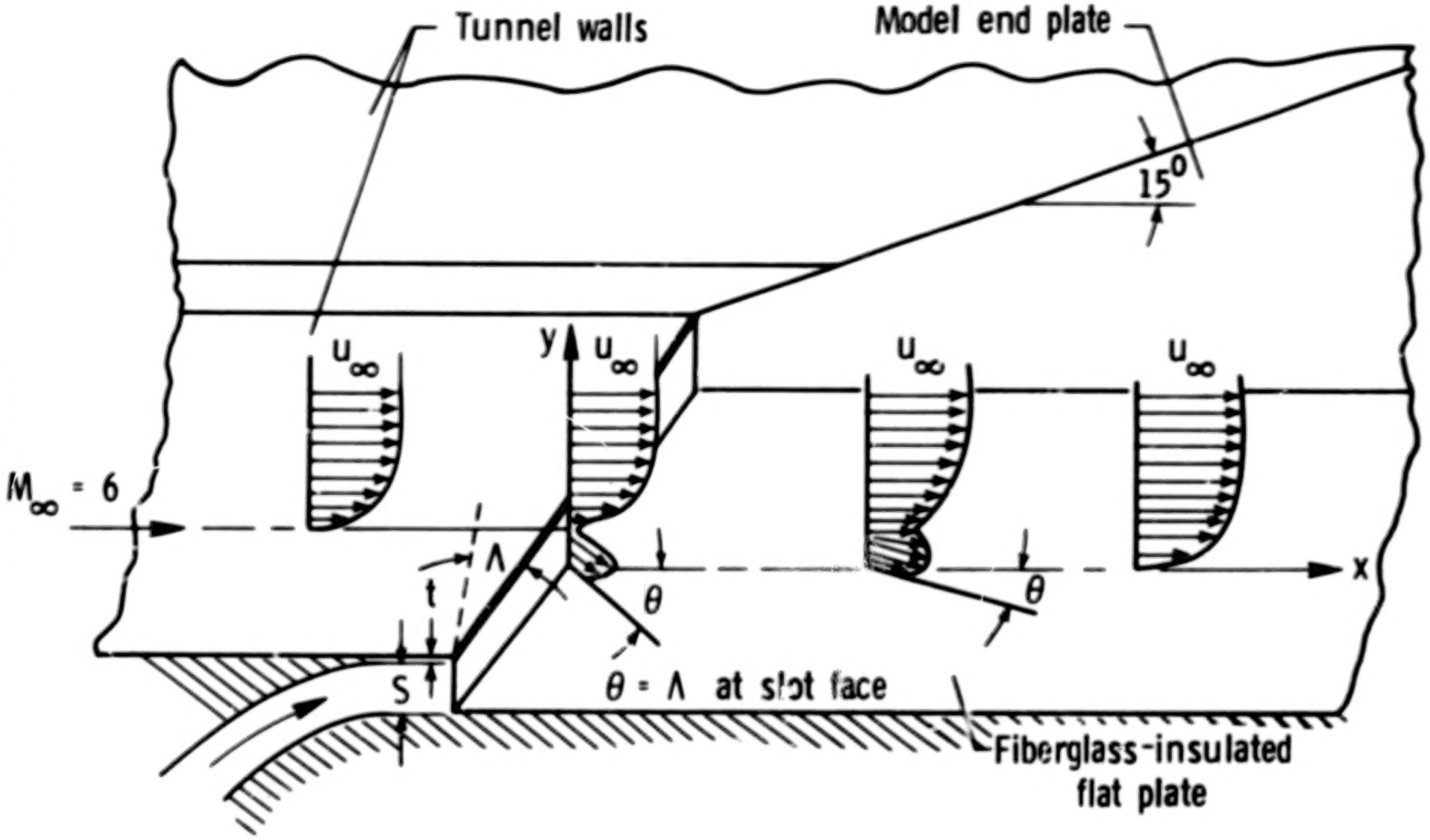

(a) Schematic of model.

Figure 1.- Sketch of experimental three-dimensional film cooling model. Dimensions are in cm.

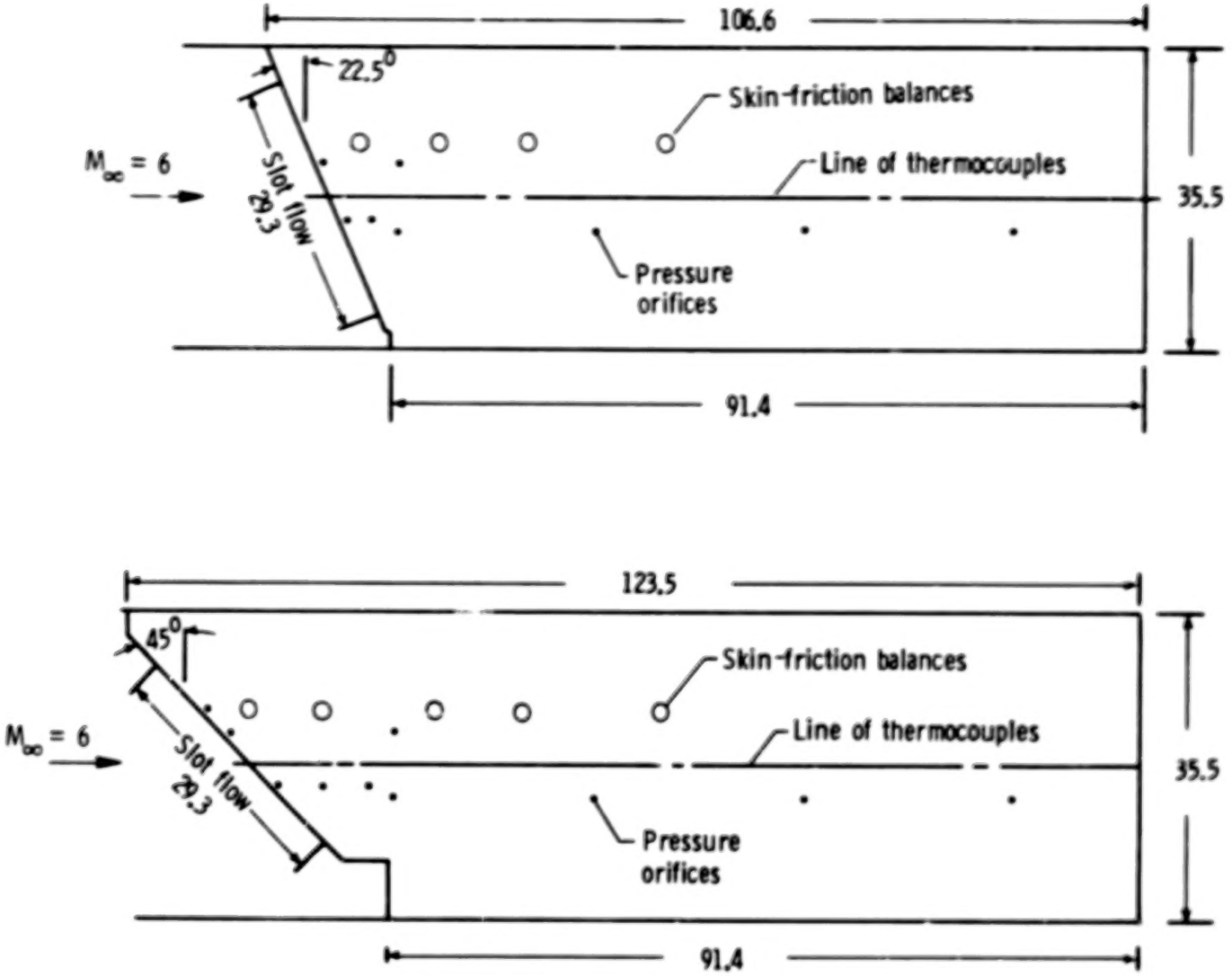

(b) Instrumentation layout.

Figure 1.- Concluded.

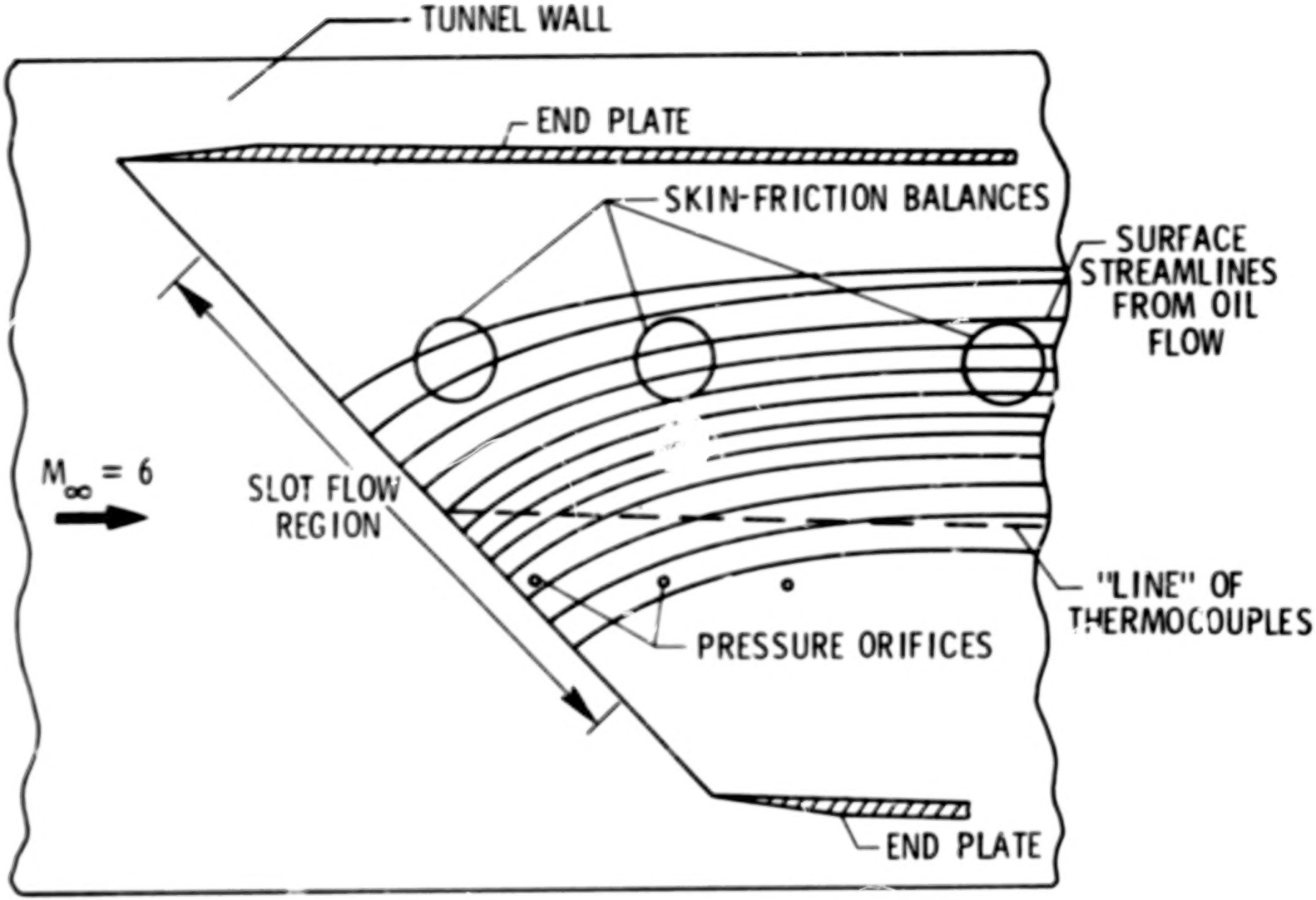

Figure 2.- Typical three-dimensional surface streamlines obtained from oil flow in instrumented region of 45° swept slot model.

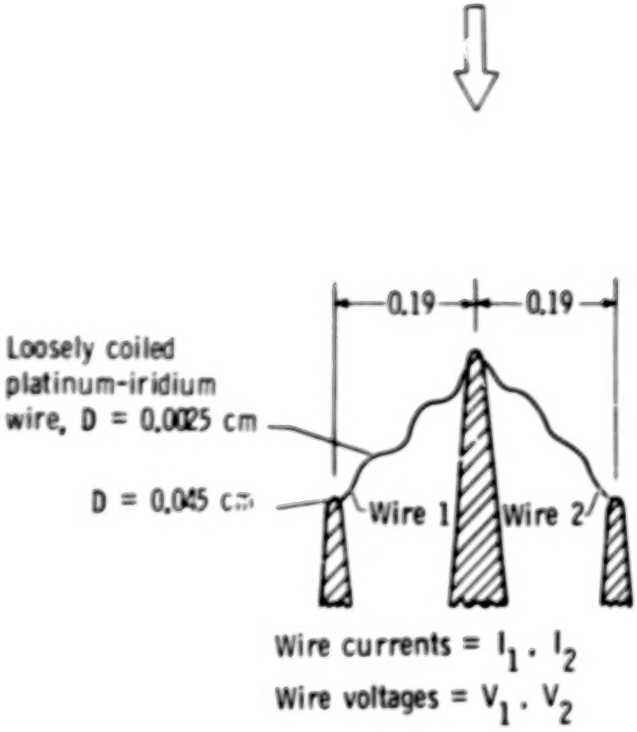

(a) Dual, swept, hot-wire flow direction probe (dimensions are in cm).

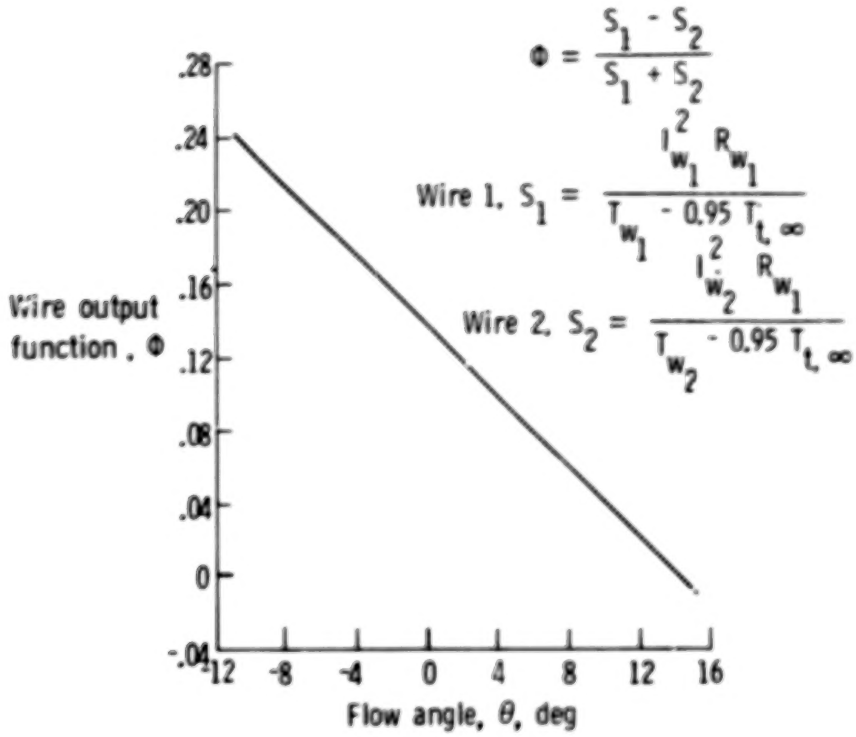

(b) Probe calibration curve (experimental).

Figure 3.- Schematic and calibration of dual, swept, hot-wire flow direction probe.

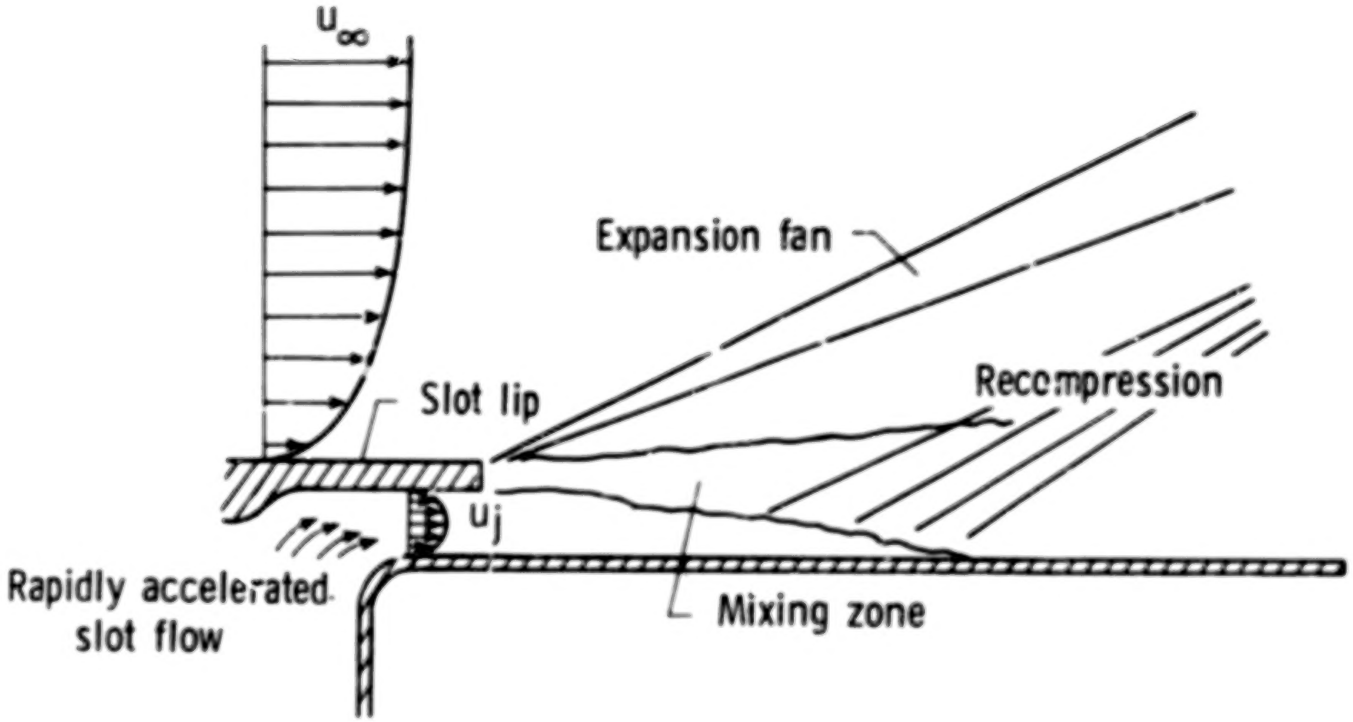

(a) Flow field downstream of slot.

Figure 4.- Flow field and pressure distribution downstream of swept slot.

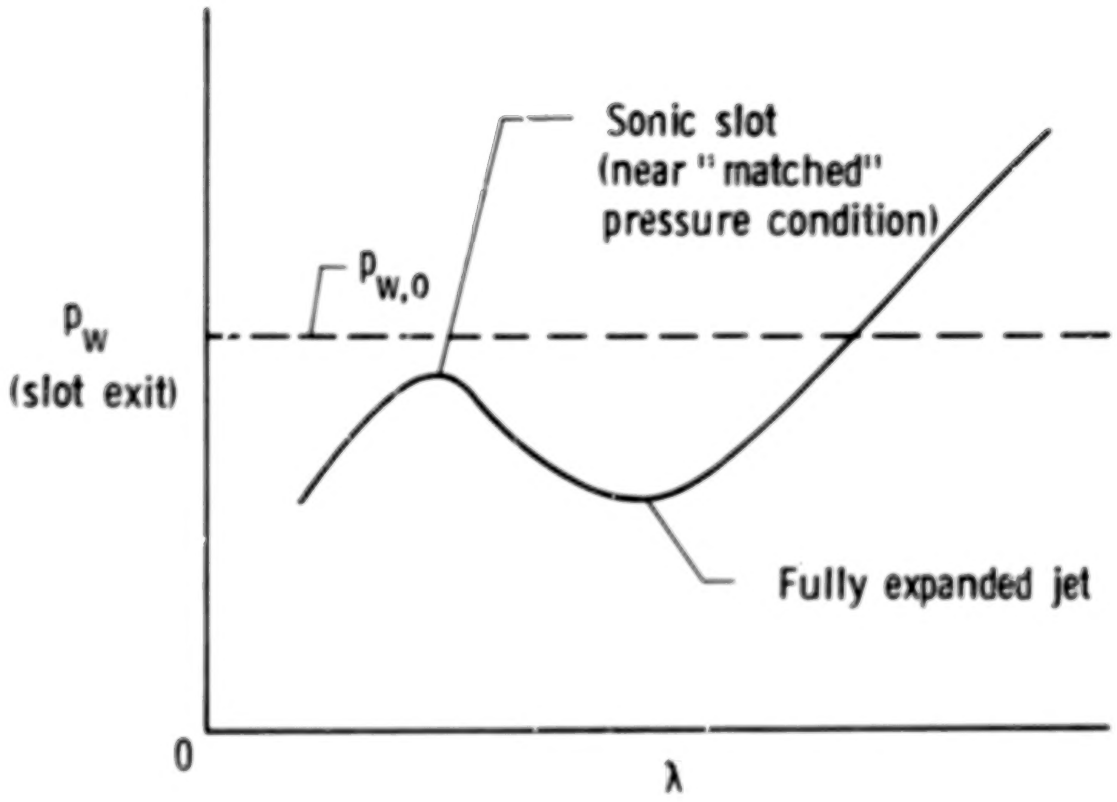

(b) Effect of mass flow rate on surface pressure near slot. x/S = 0.5.

Figure 4.- Continued.

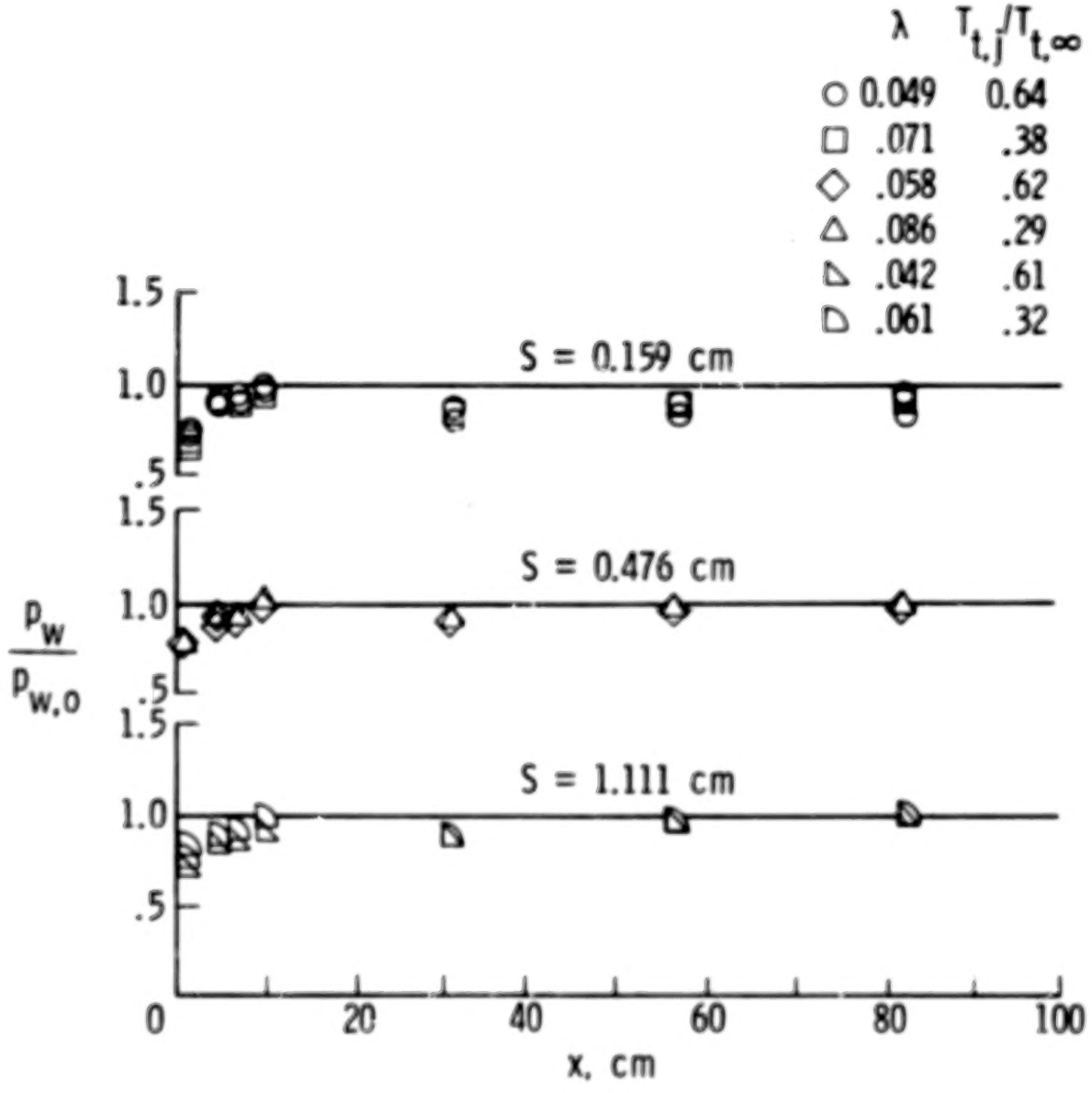

(c) Pressure distribution downstream of $\Lambda = 22.5^\circ$ slot.

Figure 4.- Continued.

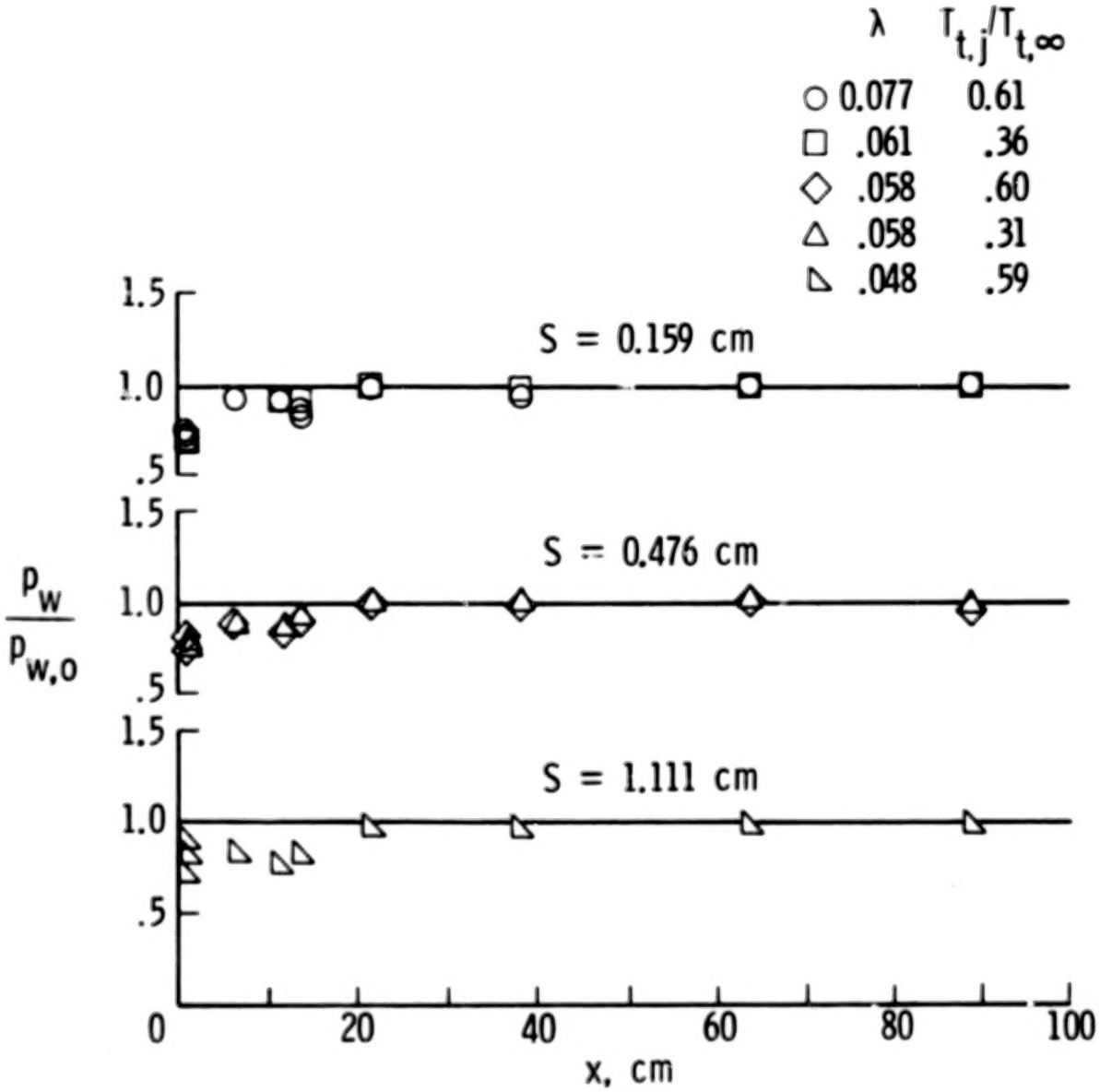

(d) Pressure distribution downstream of $\Lambda = 45^\circ$ slot.

Figure 4.- Concluded.

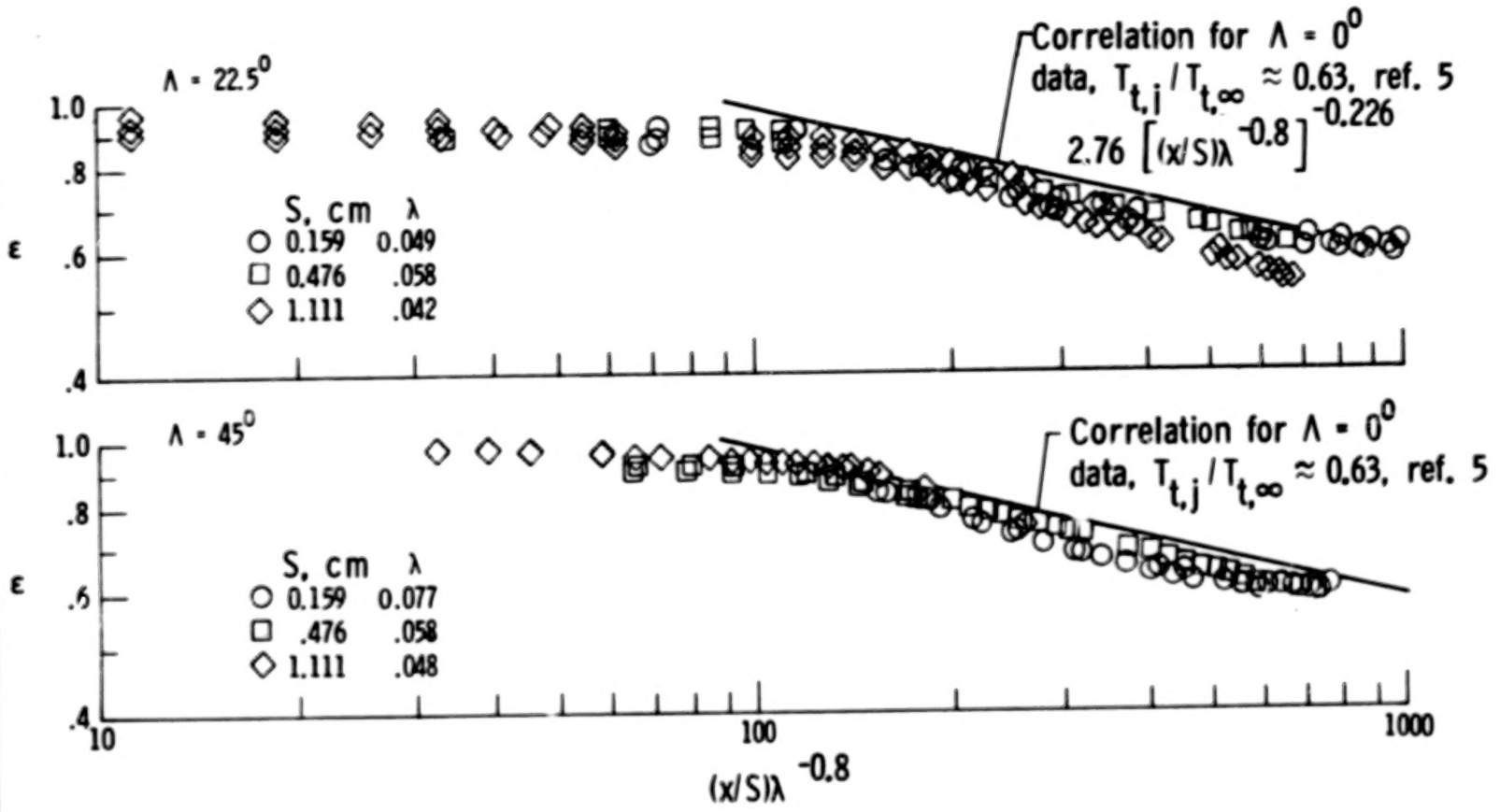

Figure 5.- Film cooling effectiveness for $T_{t,j}/T_{t,\infty} \approx 0.6$ and near "matched" pressure conditions.

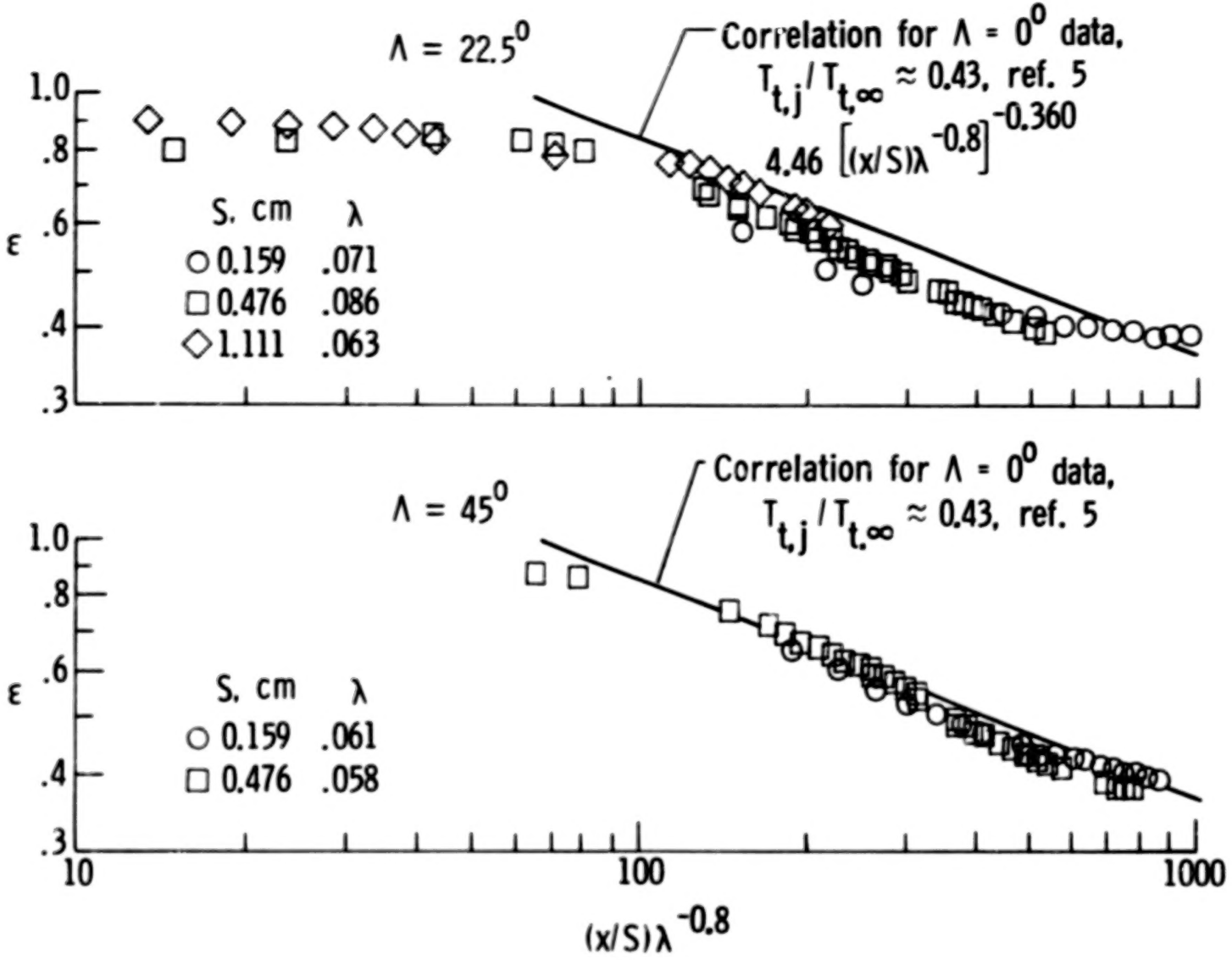

Figure 6.- Film cooling effectiveness for $T_{t,j}/T_{t,\infty} \approx 0.32$ and near "matched" pressure conditions.

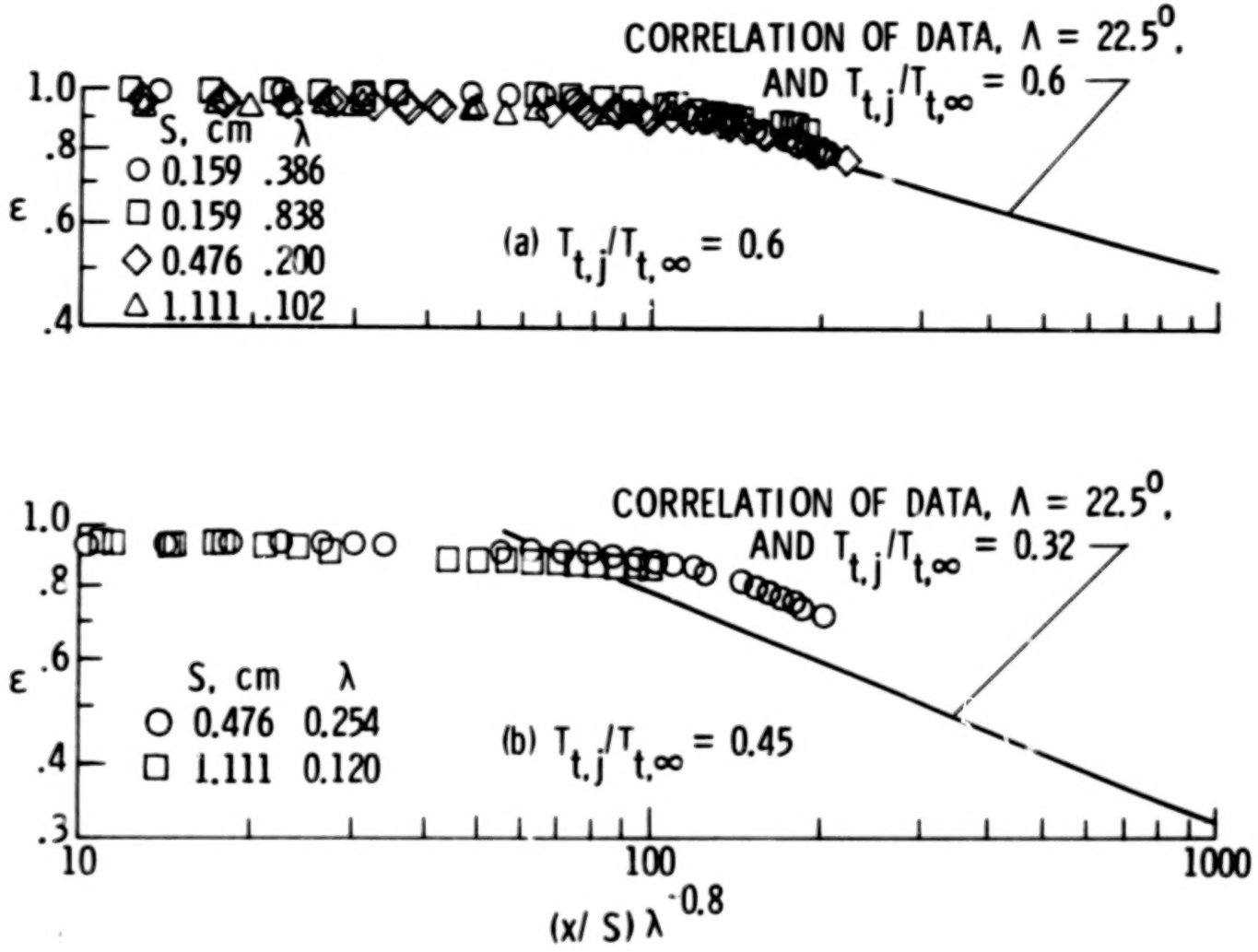

Figure 7.- Cooling effectiveness for mass flow rates greater than "matched" pressure conditions. Λ = 22.5°.

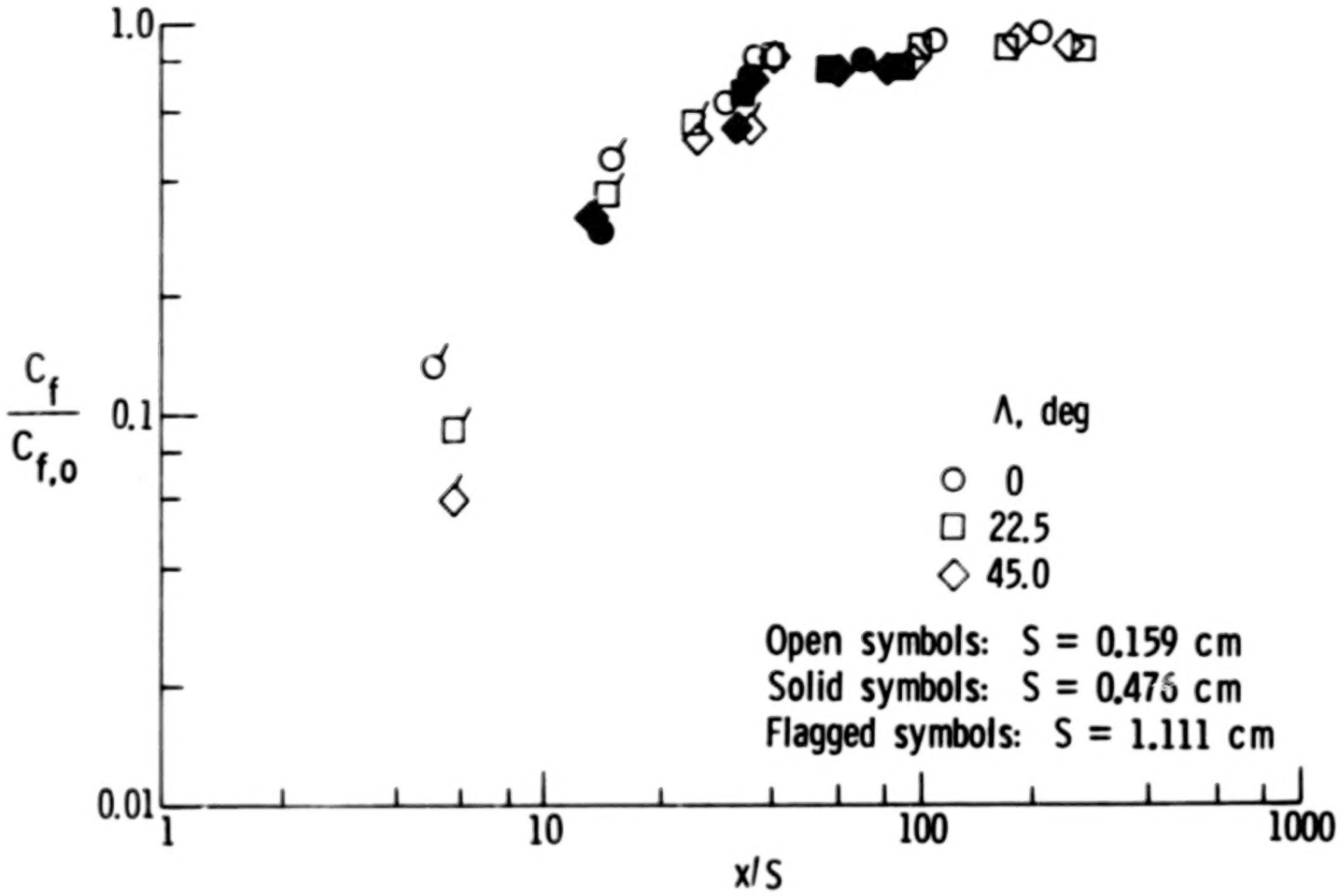

Figure 8.- Skin friction downstream of slot for "matched" pressure conditions. $0.042 \leq \lambda \leq 0.077$.

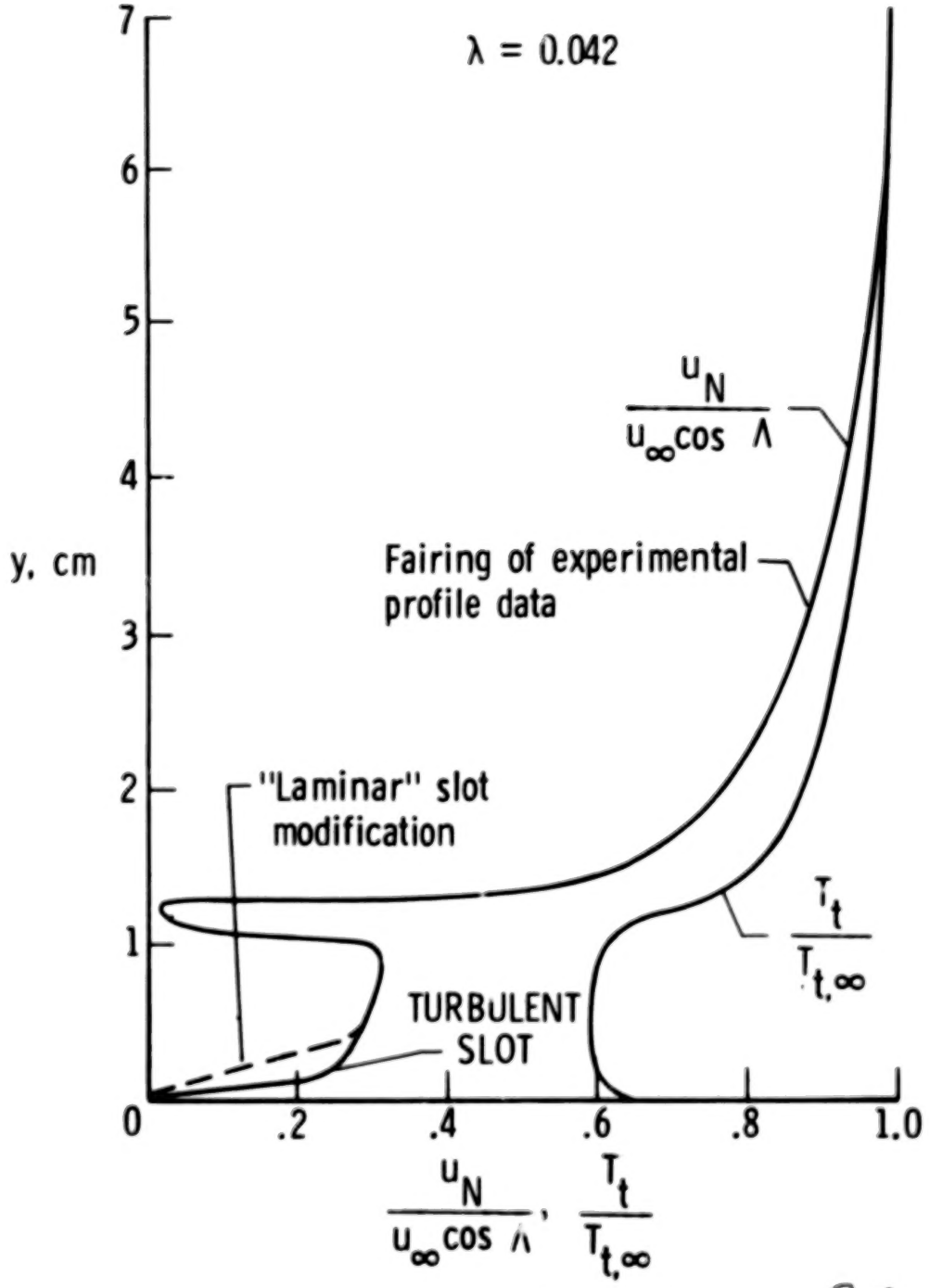

(a) $\Lambda = 22.5^\circ$; $T_{t,j}/T_{t,\infty} = 0.6$.

32.

Figure 9.- Initial boundary-layer and slot profiles (normal to slot) used in the finite-difference calculations. S = 1.111 cm.

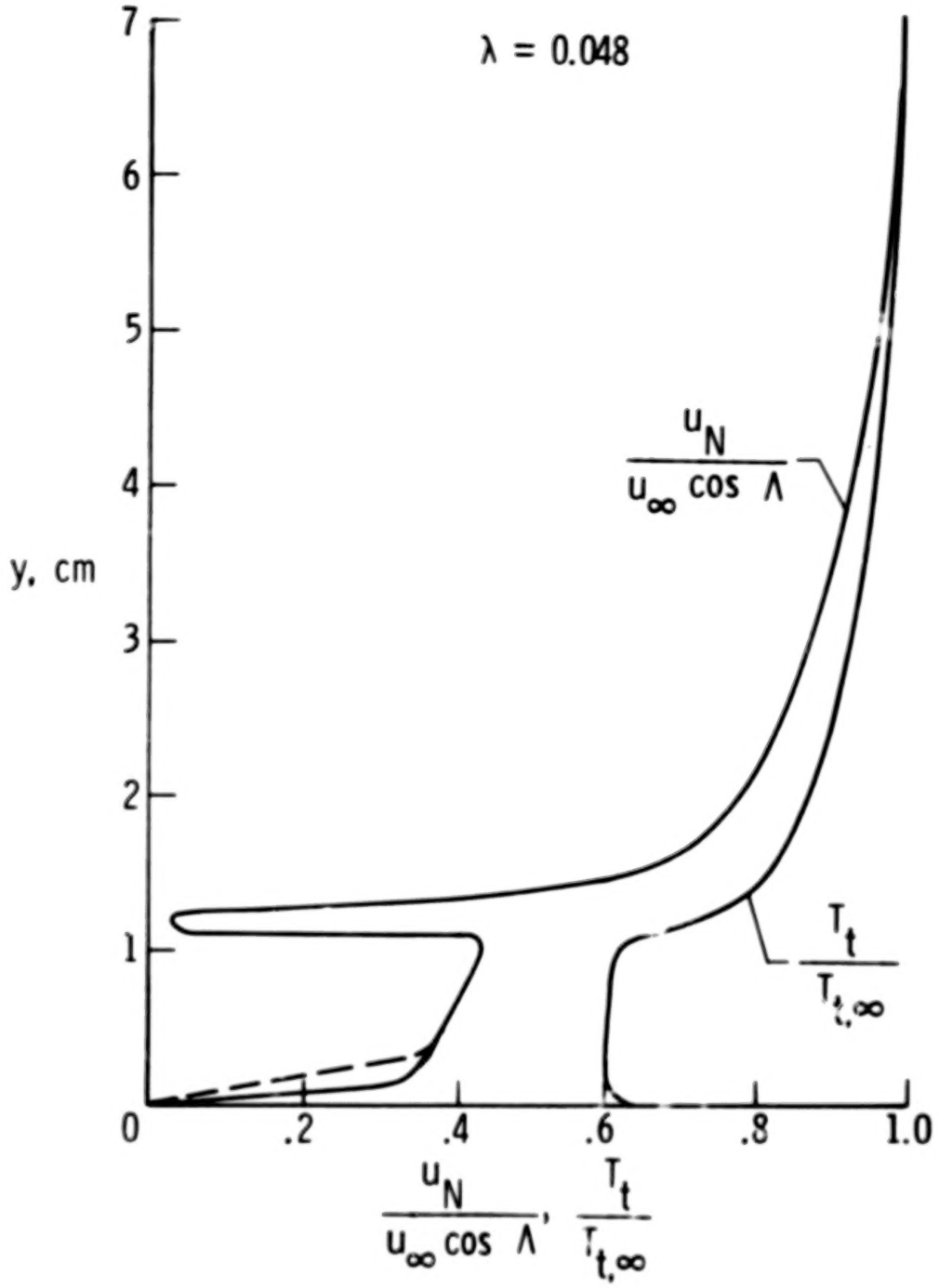

(b) $\Lambda = 45°$; $T_{t,j}/T_{t,\infty} = 0.6$.

Figure 9.- Continued.

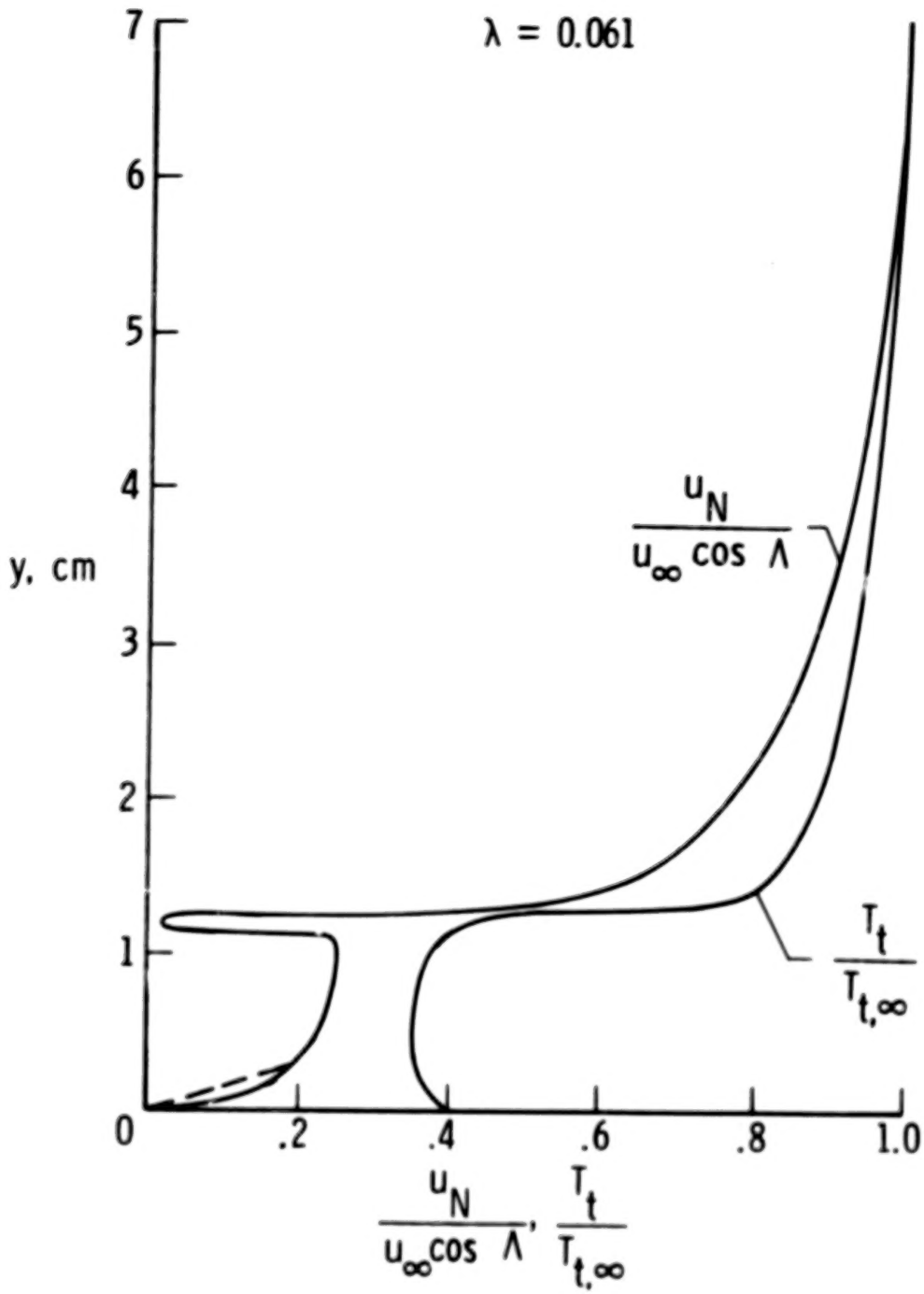

(c) $\Lambda = 22.5^\circ$; $T_{t,j}/T_{t,\infty} = 0.32$.

Figure 9.- Concluded.

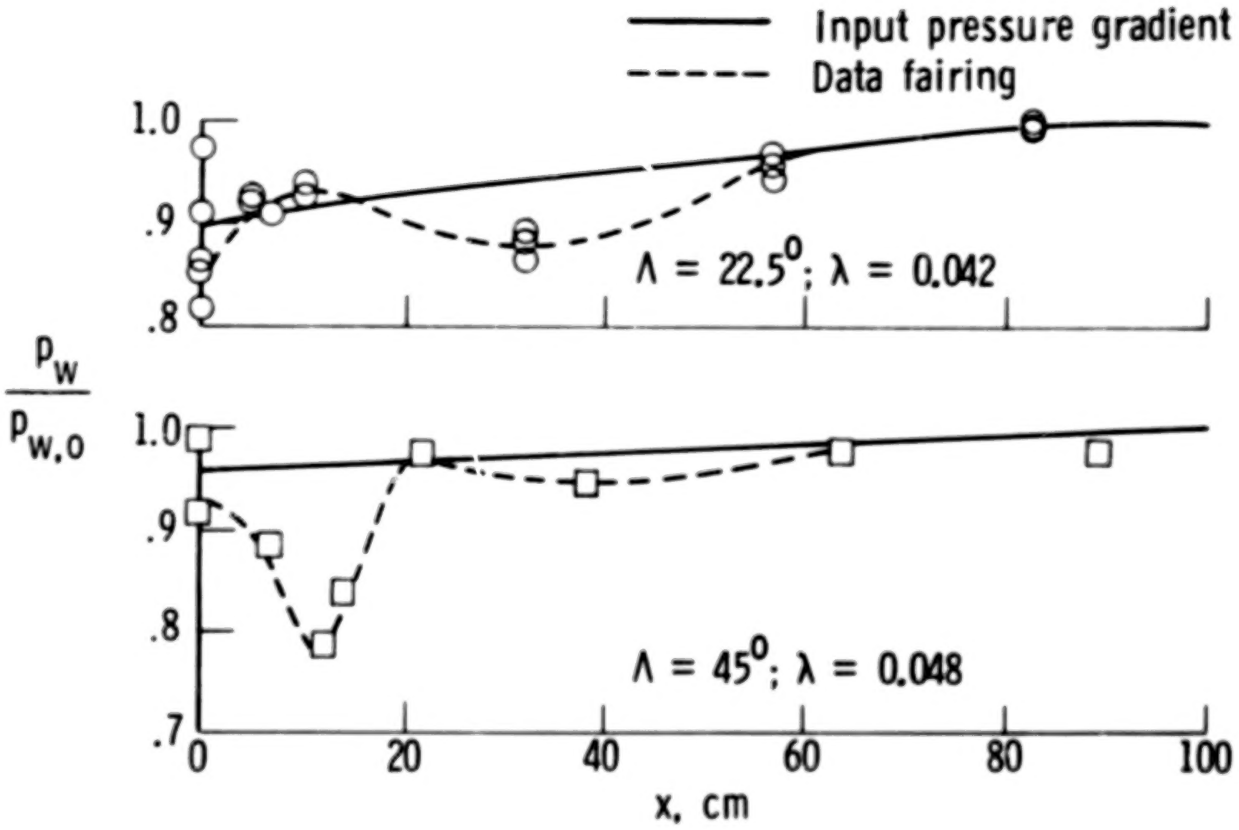

Figure 10.- Input pressure gradients for finite-difference program. $T_{t,j}/T_{t,\infty} = 0.6$; S = 1.111 cm.

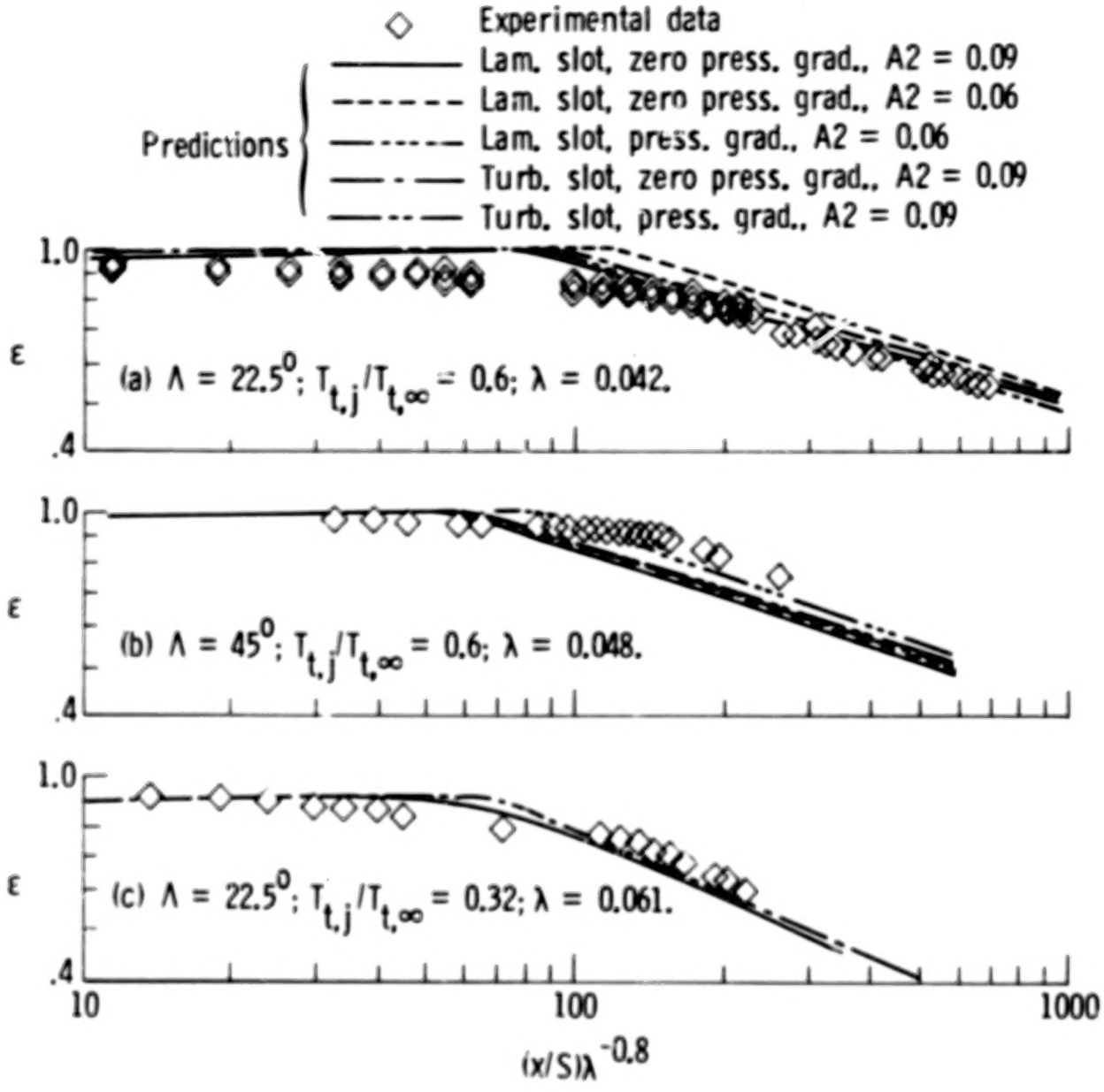

Figure 11.- Comparison of finite-difference predictions with experimental cooling-effectiveness data. S = 1.111 cm.

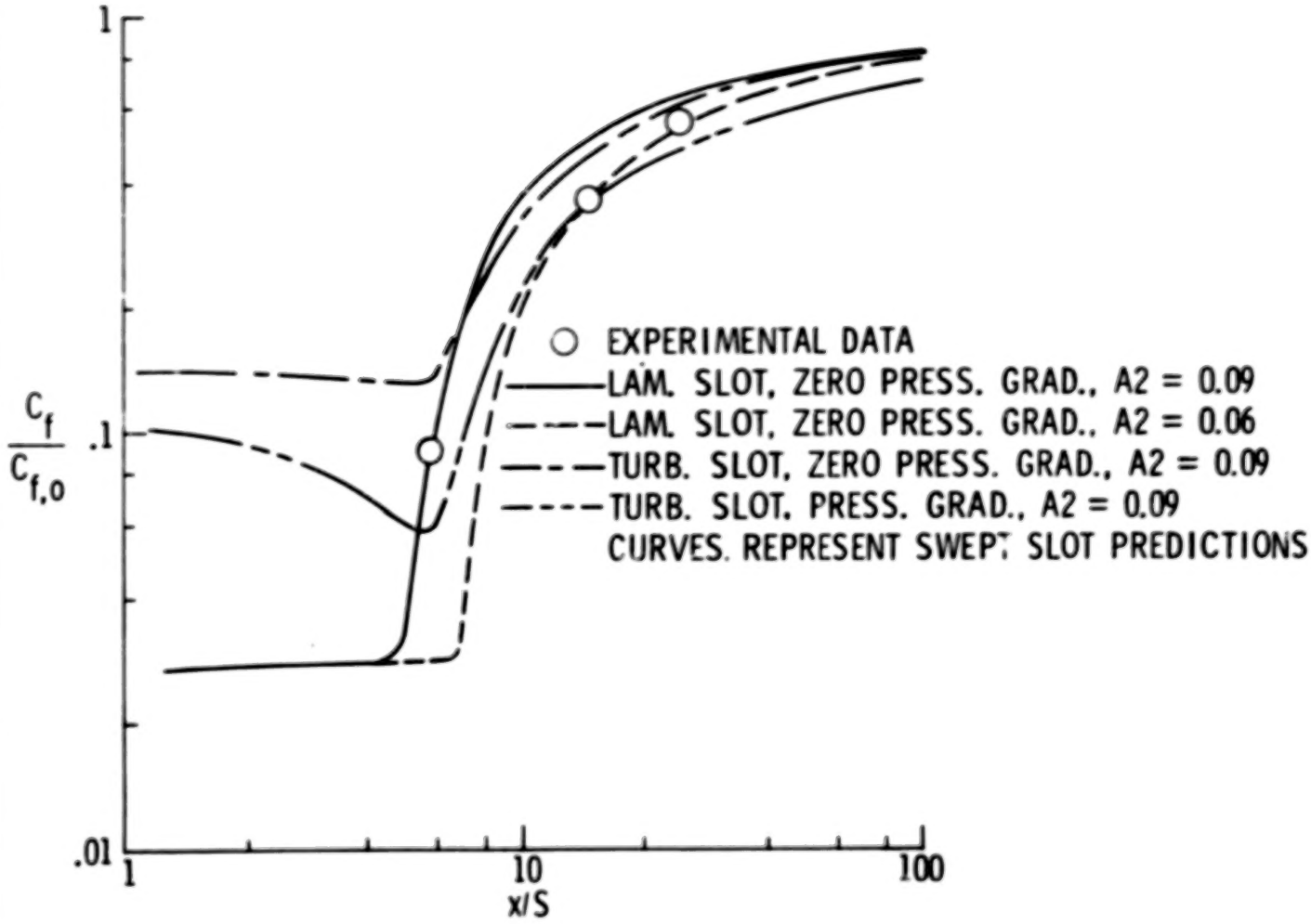

(a) $\Lambda = 22.5^{\circ}$; $T_{t,j}/T_{t,\infty} = 0.6$; $\lambda = 0.042$.

Figure 12.- Comparison of finite-difference predictions with experimental skin-friction data. S = 1.111 cm.

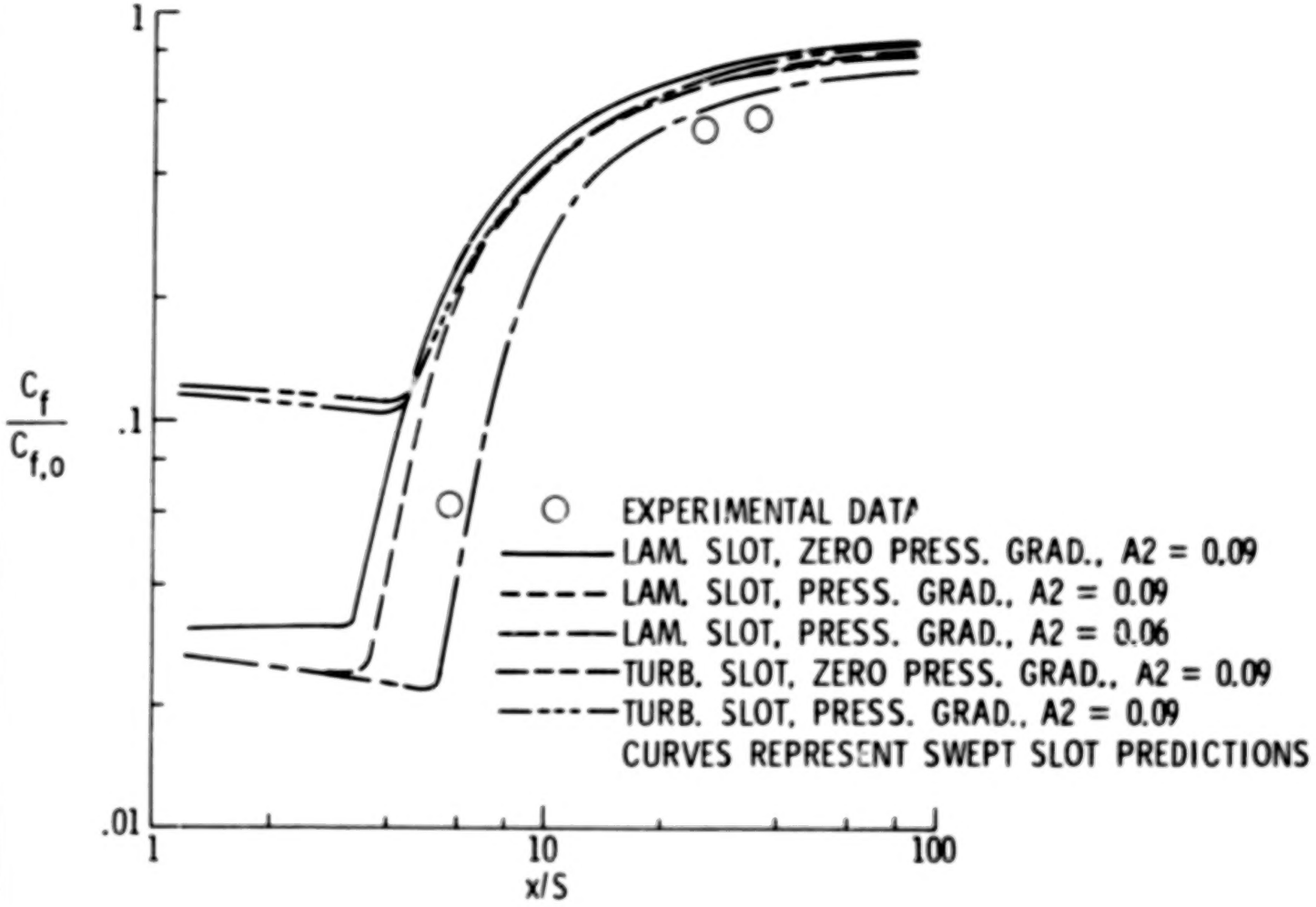

(b) $\Lambda = 45°$; $T_{t,j}/T_{t,\infty} = 0.6$; $\lambda = 0.048$.

Figure 12.- Concluded.

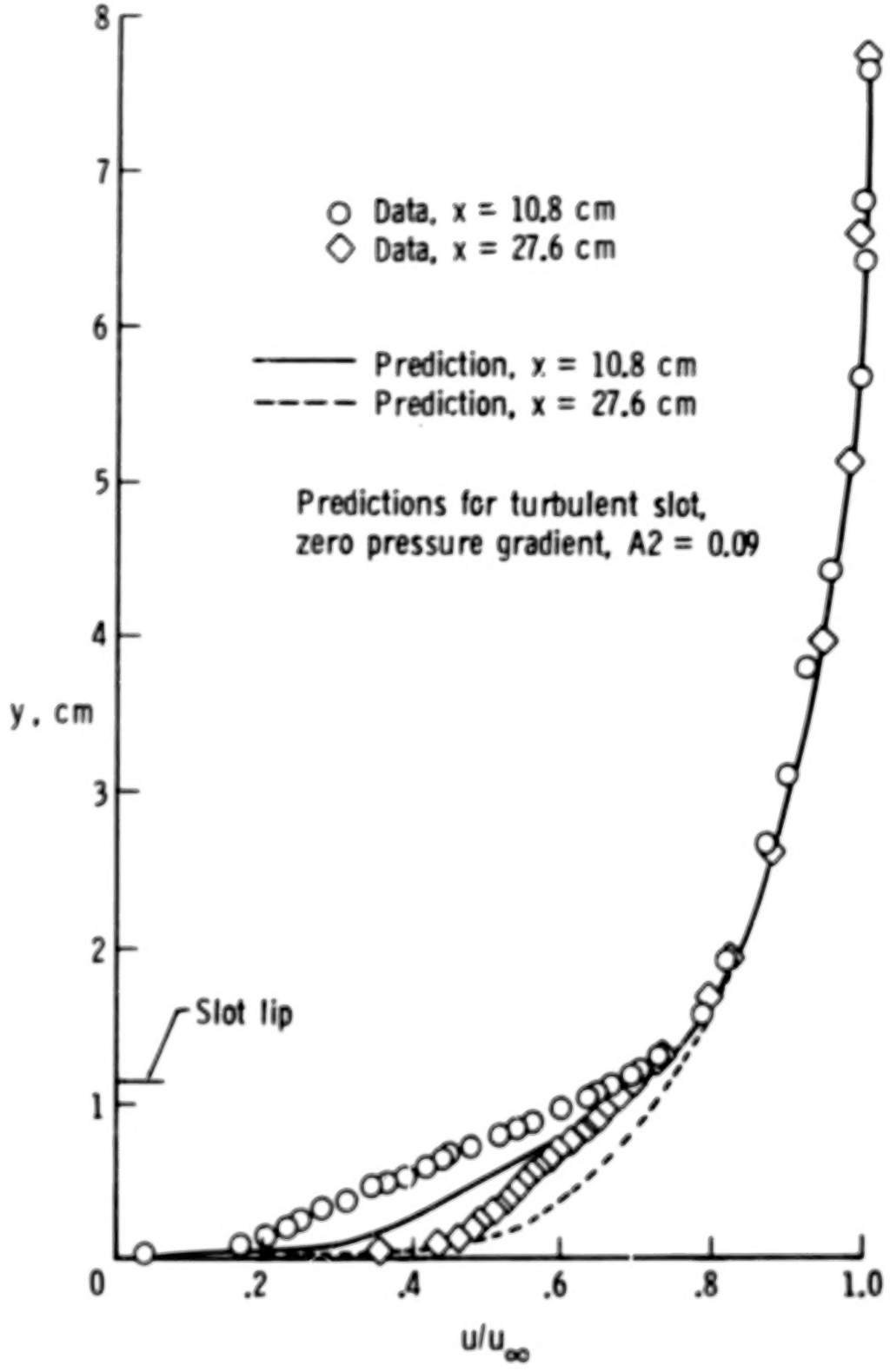

(a) $\Lambda = 0^{\circ}$; $T_{t,j}/T_{t,\infty} = 0.6$; $\lambda = 0.047$.

Figure 13.- Comparison of finite-difference predictions with experimental velocity profiles. S = 1.111 cm.

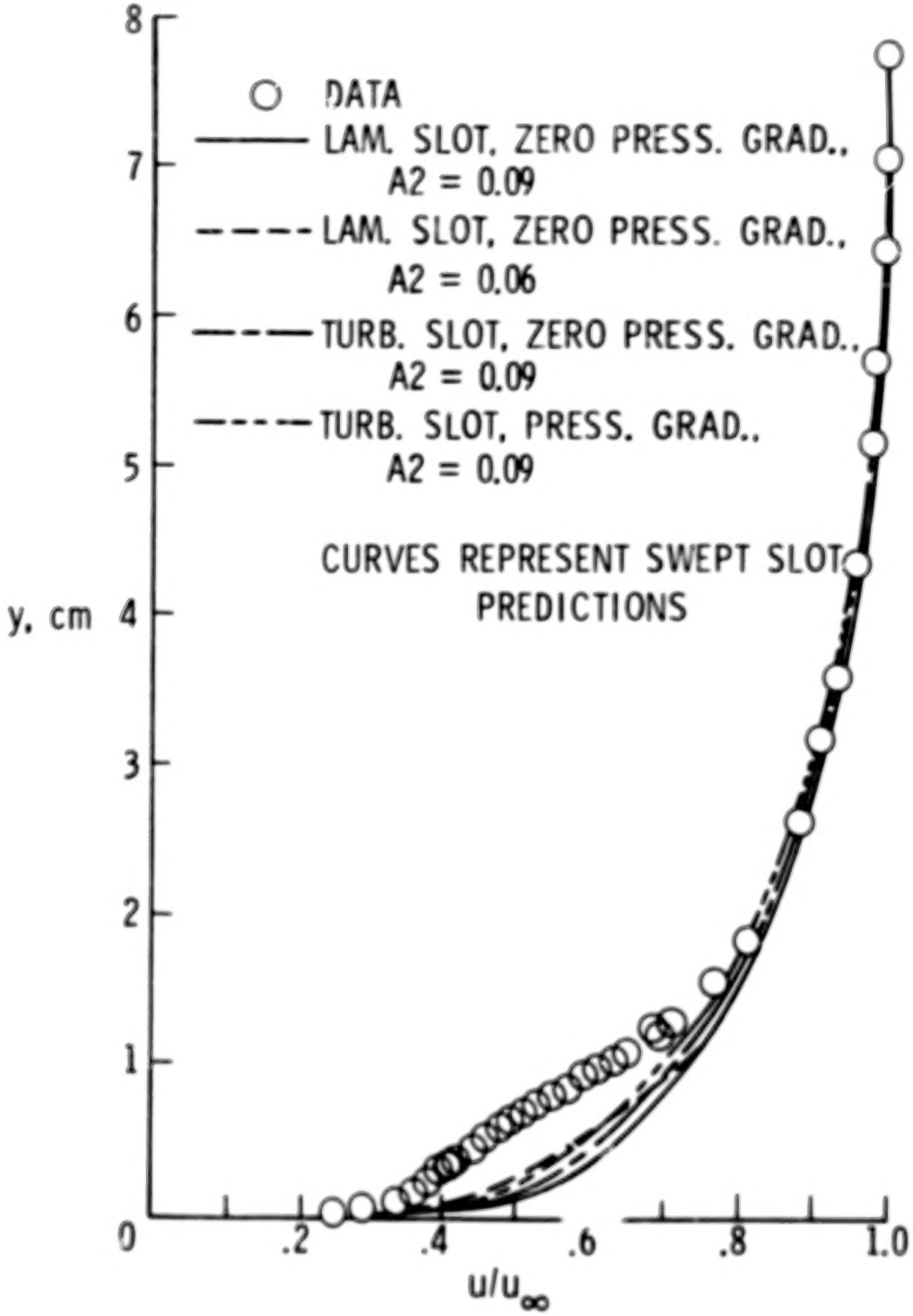

(b) $\Lambda = 22.5°$; $T_{t,j}/T_{t,\infty} = 0.6$; $\lambda = 0.042$; $x = 21.1$ cm.

Figure 13.- Continued.

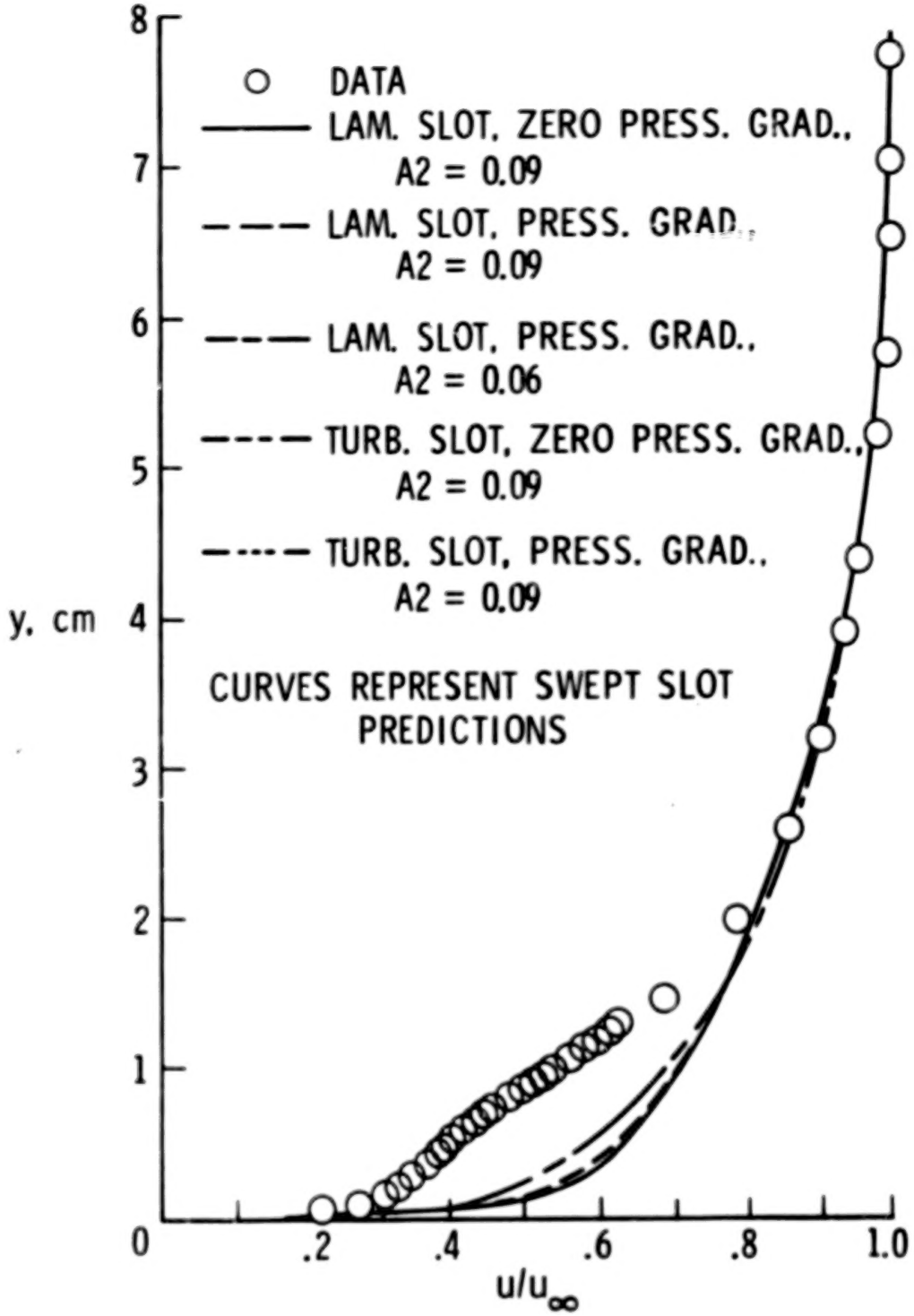

(c) $\Lambda = 45^{\circ}$; $T_{t,j}/T_{t,\infty} = 0.6$; $\lambda = 0.048$; $x = 23$ cm.

Figure 13.- Continued.

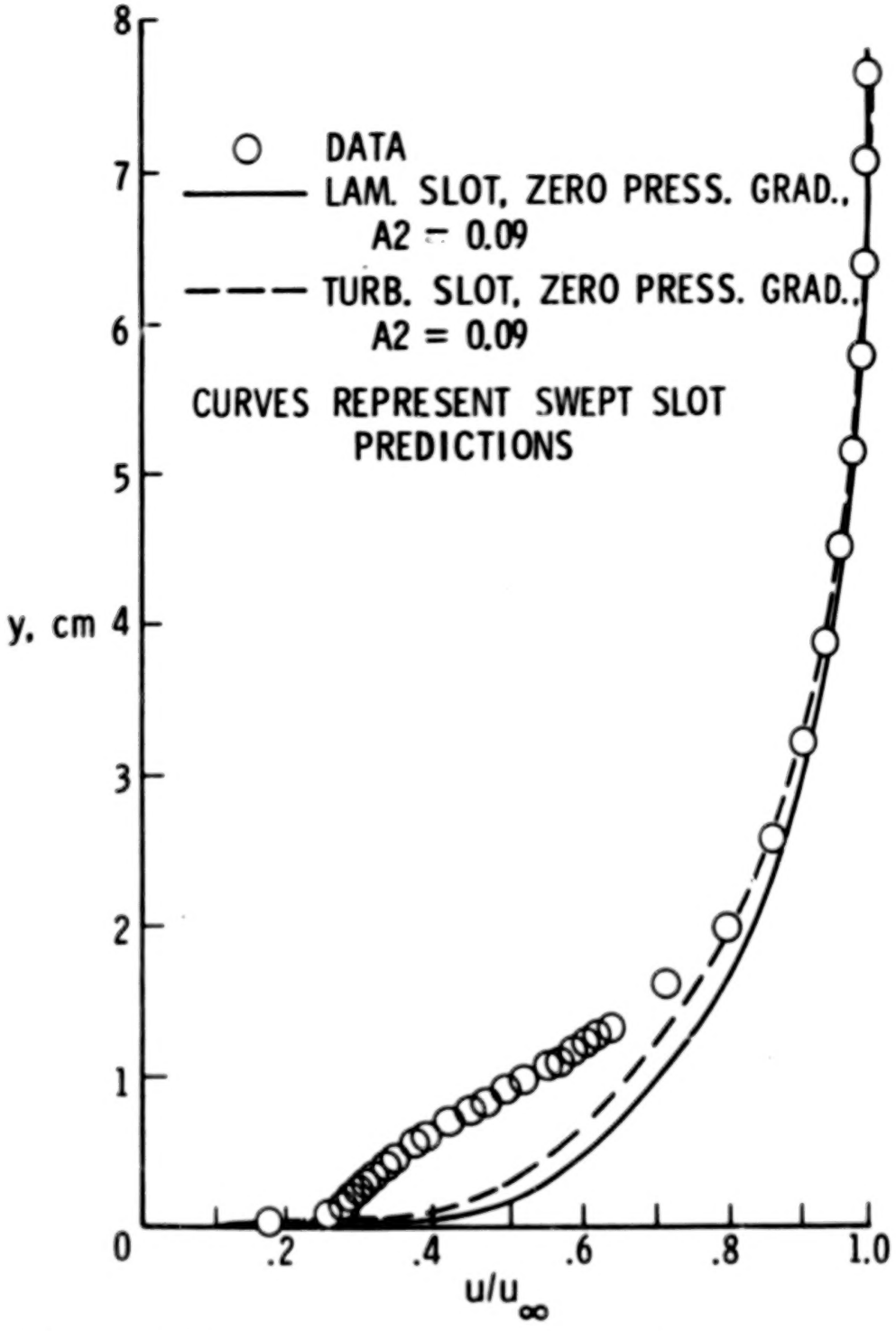

(d) $\Lambda = 22.5^{\circ}$; $T_{t,j}/T_{t,\infty} = 0.32$; $\lambda = 0.061$; $x = 21.1$ cm.

Figure 13.- Concluded.

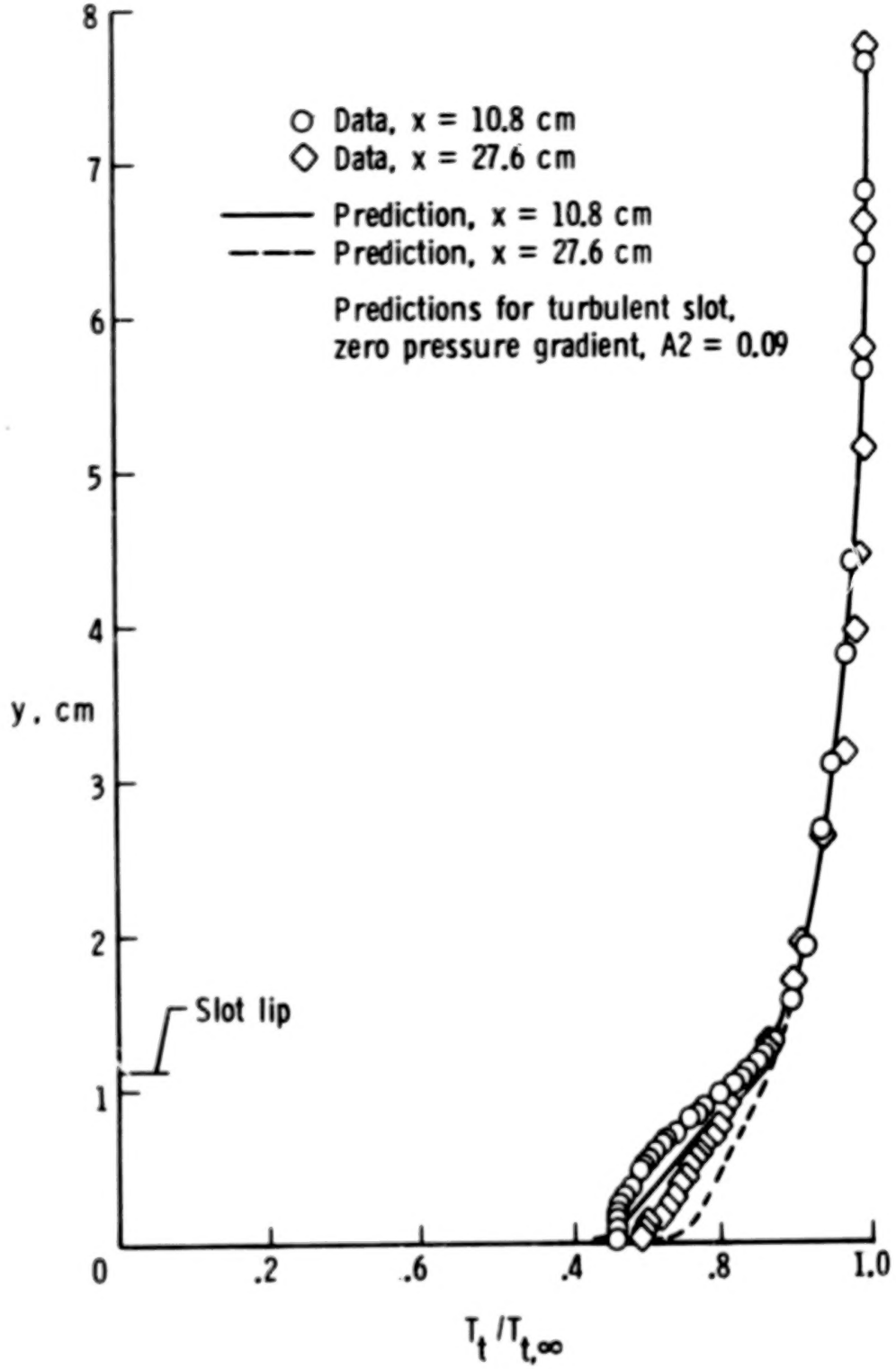

(a) $\Lambda = 0^{o}$; $T_{t,j}/T_{t,\infty} = 0.6$; $\lambda = 0.047$.

Figure 14.- Comparison of finite-difference predictions with experimental total temperature profiles. S = 1.111 cm.

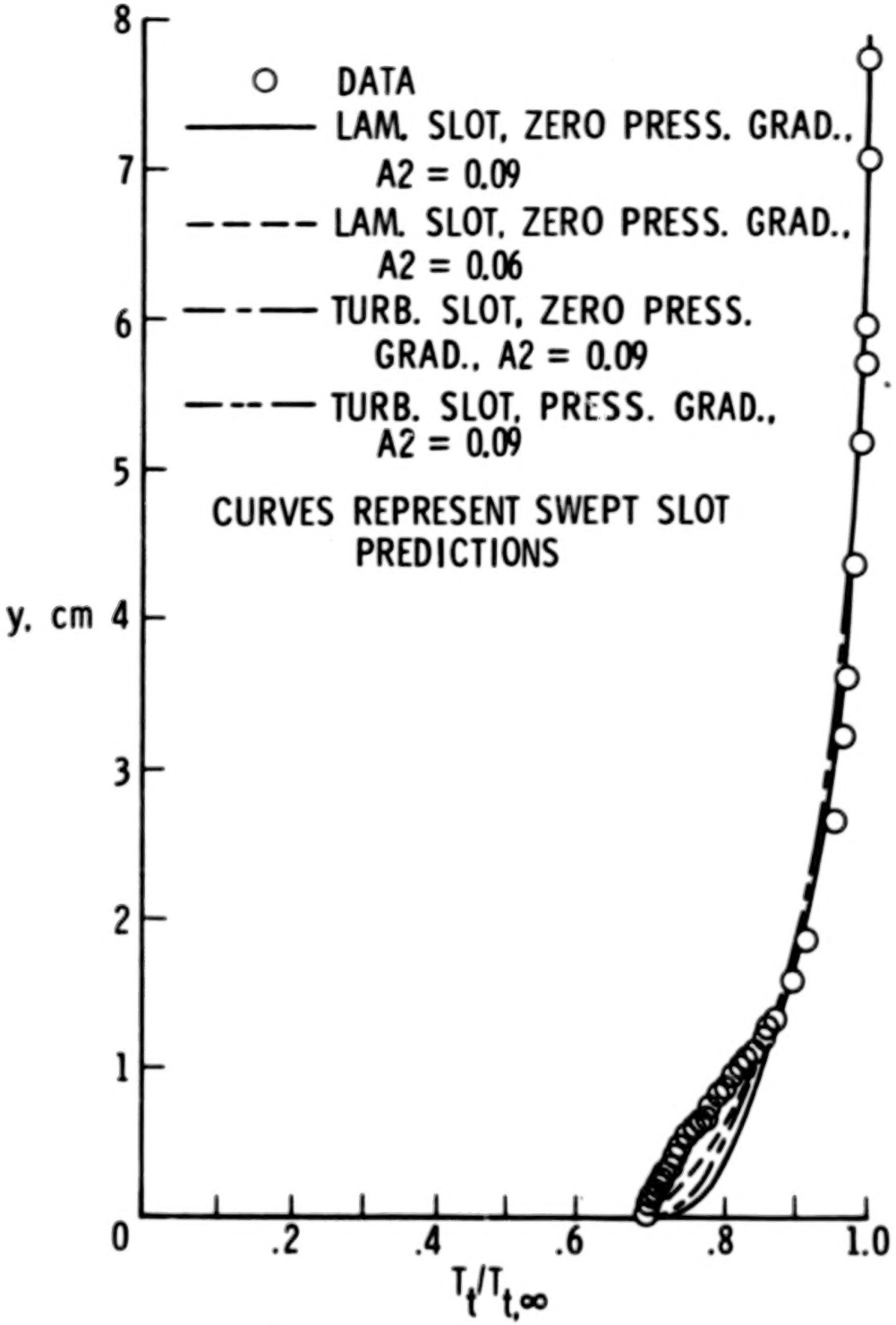

(b) $\Lambda = 22.5°$; $T_{t,j}/T_{t,\infty} = 0.6$; $\lambda = 0.042$; $x = 21.1$ cm.

Figure 14.- Continued.

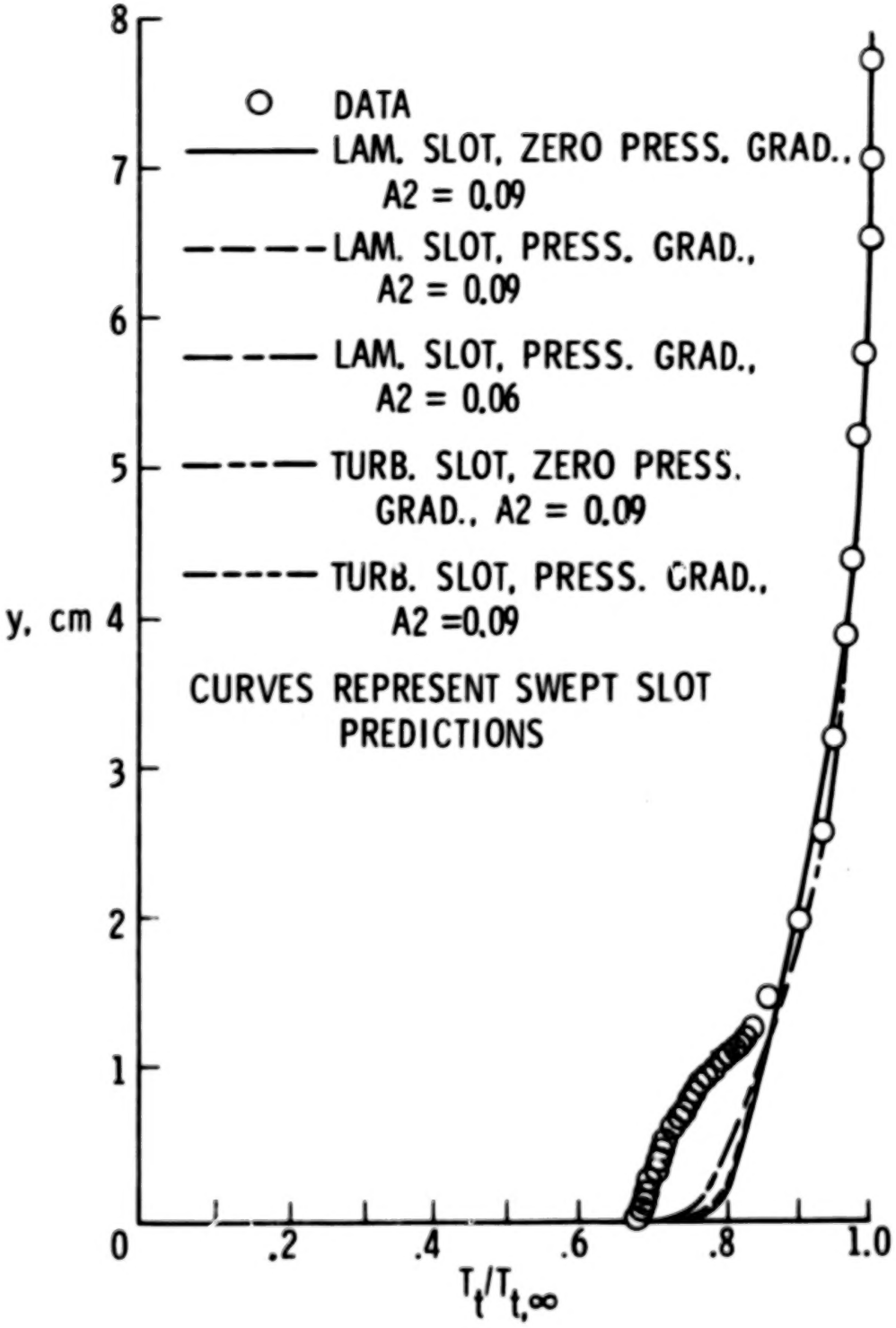

(c) $\Lambda = 45^{\circ}$; $T_{t,j}/T_{t,\infty} = 0.6$; $\lambda = 0.048$; $x = 23$ cm.

Figure 14.- Continued.

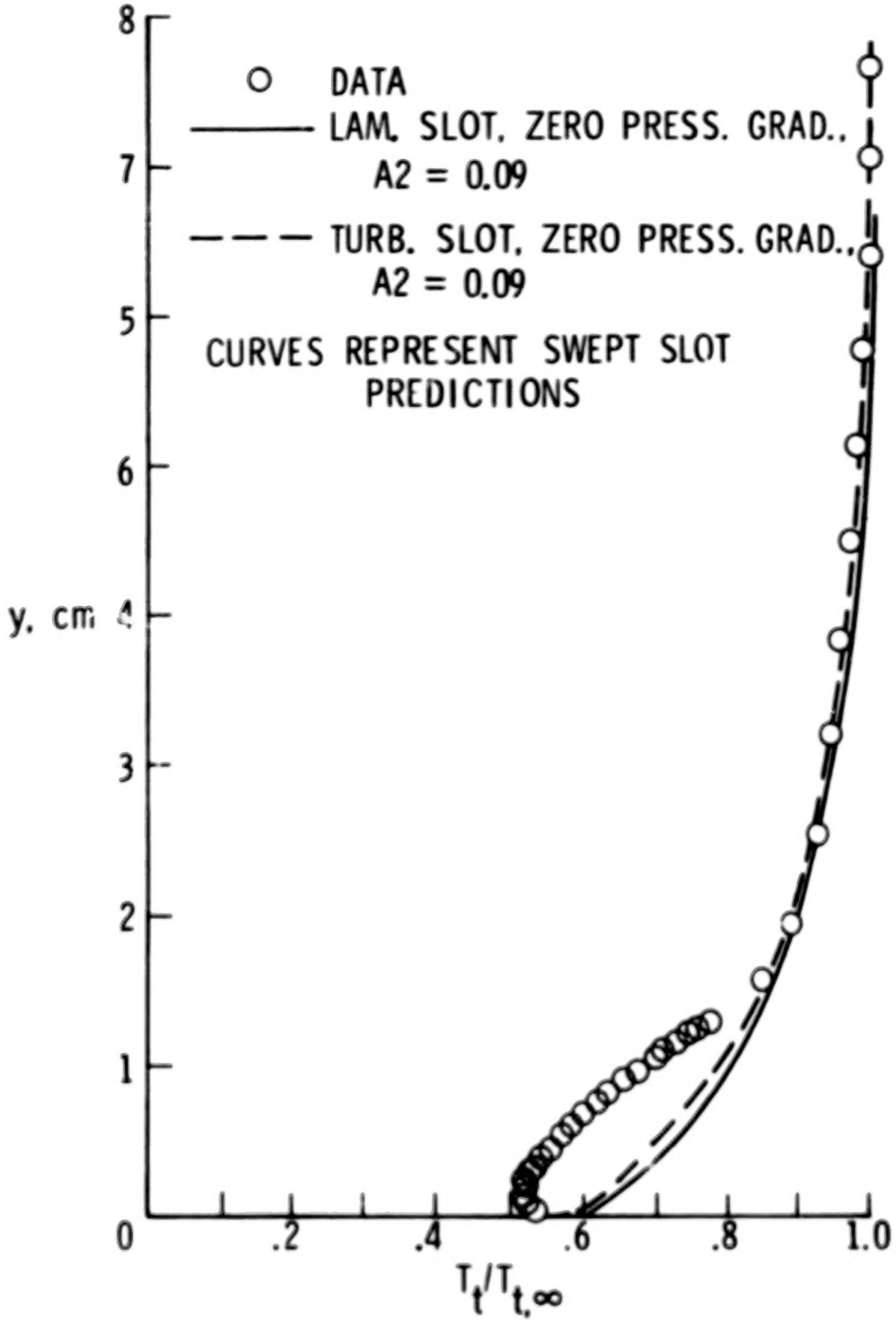

(d) $\Lambda = 22.5^{\circ}$; $T_{t,j}/T_{t,\infty} = 0.32$; $\lambda = 0.061$; $x = 21.1$ cm.

Figure 14.- Concluded.

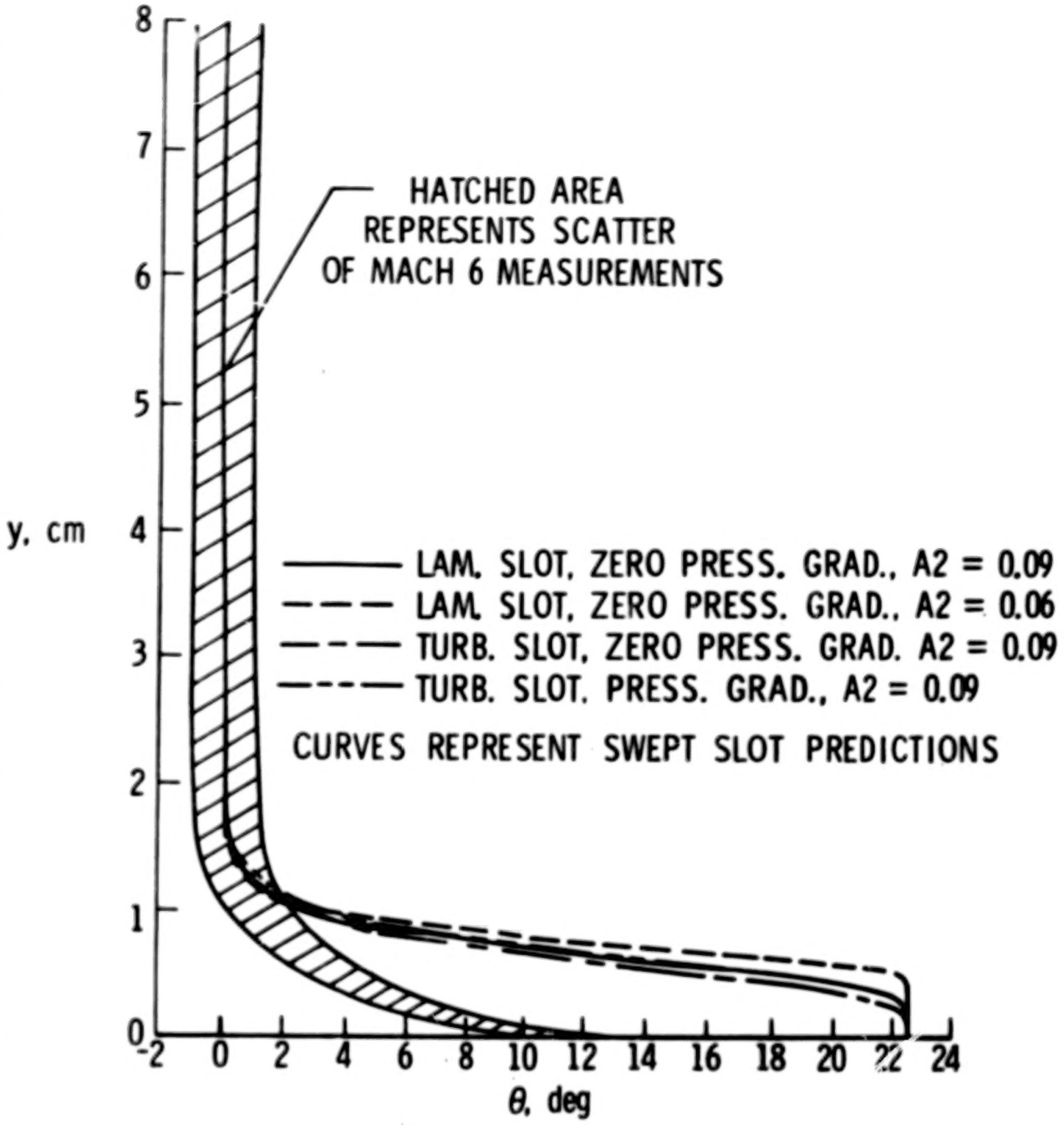

(a) $\Lambda = 22.5^{\circ}$; $T_{t,j}/T_{t,\infty} = 0.06$; $\lambda = 0.042$; $x = 5.40$ cm.

Figure 15.- Comparison of finite-difference predictions with swept-wire flow angularity measurements. S = 1.111 cm.

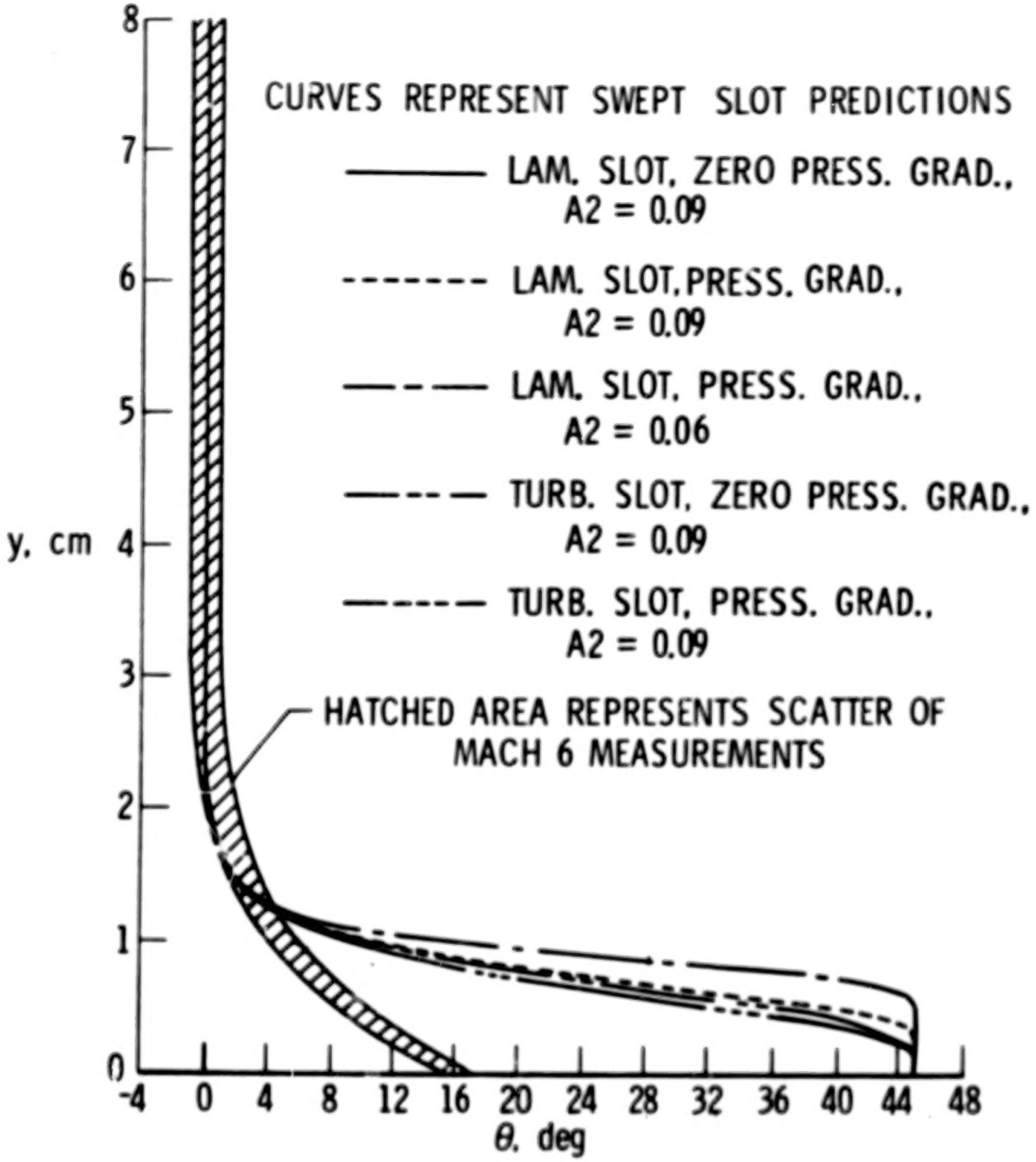

(b) $\Lambda = 45^{\circ}$; $T_{t,j}/T_{t,\infty} = 0.6$; $\lambda = 0.048$; $x = 8.26$ cm.

Figure 15.- Concluded.

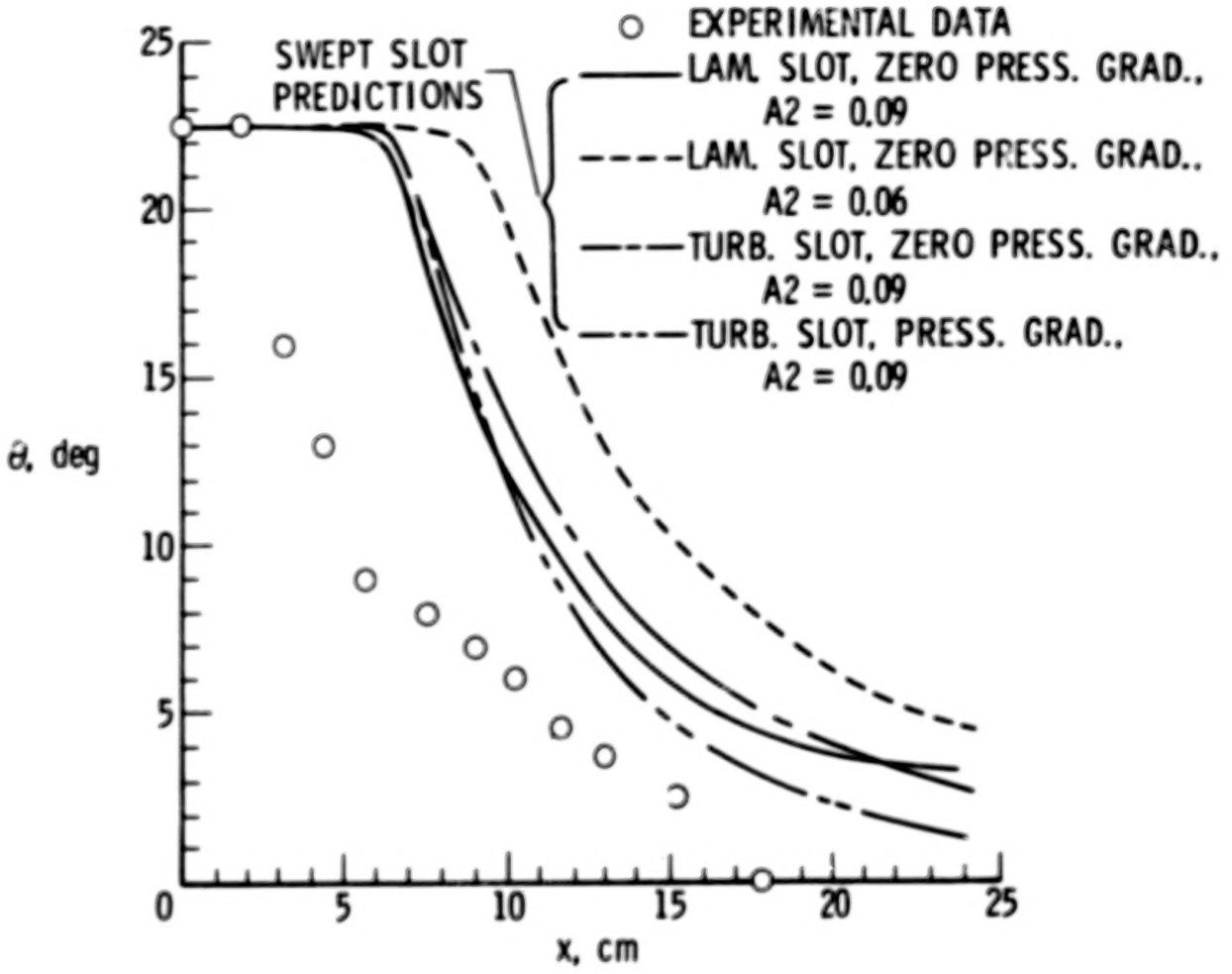

(a) $\Lambda = 22.5^{\circ}$; $\lambda = 0.042$.

Figure 16.- Surface flow angle for swept slot injection. $S = 1.111$ cm; $T_{t,j}/T_{t,\infty} = 0.6$.

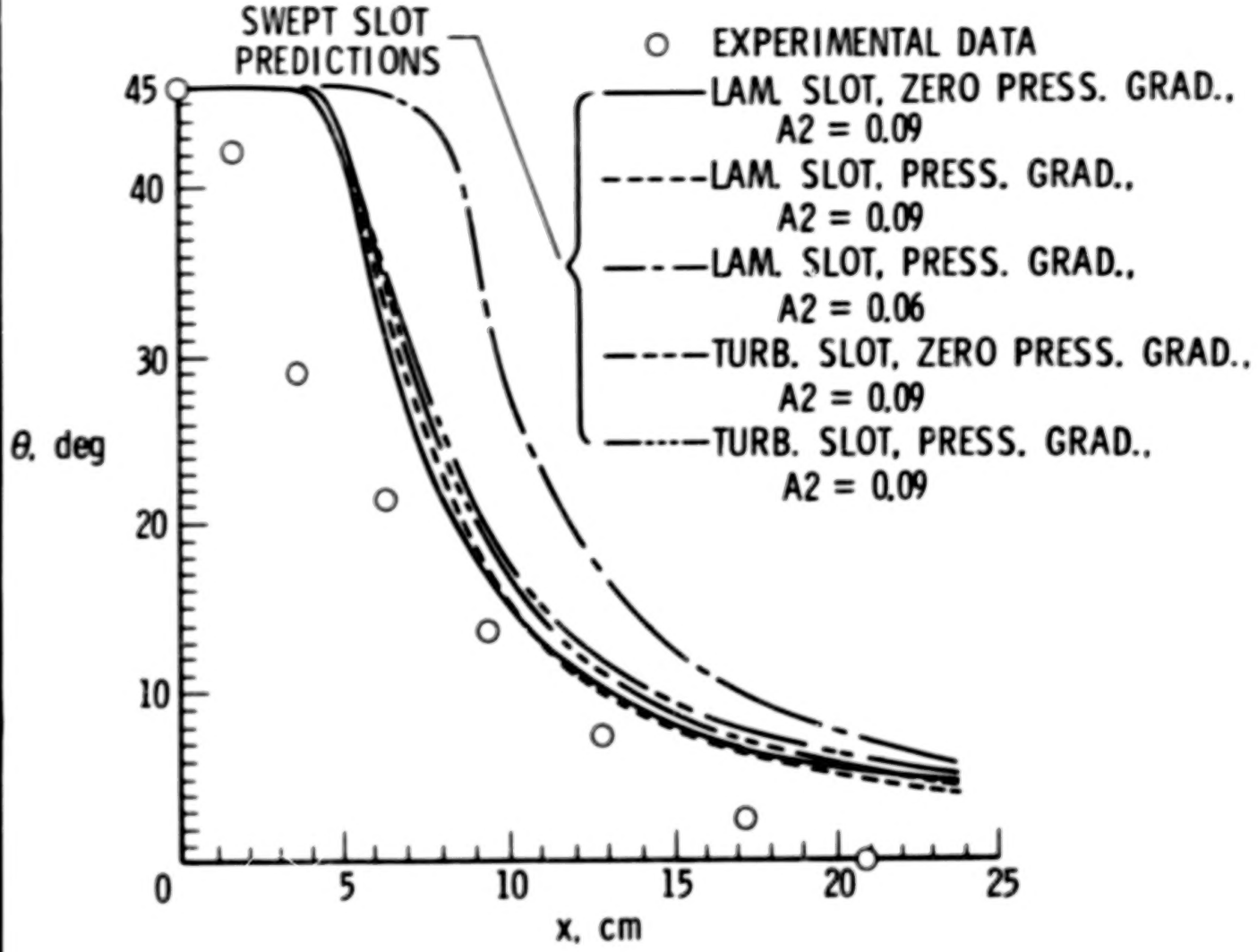

(b) $\Lambda = 45°$; $\lambda = 0.048$.

Figure 16.- Concluded.

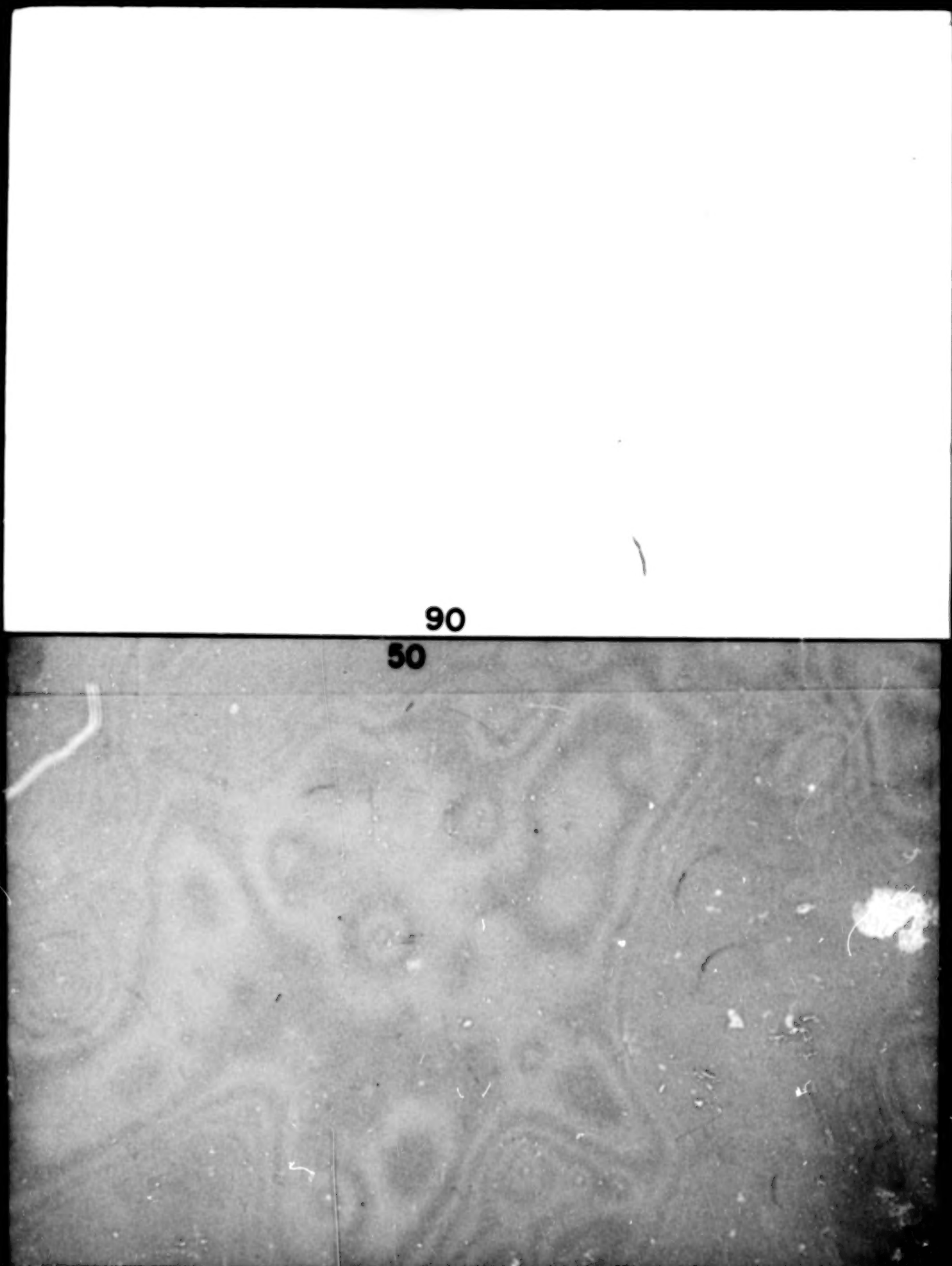
90
50

END

5.19 78